Fall 2022

Decellularization Strategies of Naturally Derived Biomaterials for Tissue Engineering Applications

Julia Elizabeth Hohn

DECELLULARIZATION STRATEGIES OF NATURALLY DERIVED BIOMATERIALS FOR TISSUE ENGINEERING APPLICATIONS

By

Julia Elizabeth Hohn

Bachelor of Science
University of Arkansas, 2014

Master of Science
University of South Carolina, 2019

Submitted in Partial Fulfillment of the Requirements

For the Degree of Doctor of Philosophy in

Biomedical Science

College of Arts and Sciences

University of South Carolina

2022

Accepted by:

Wayne Carver, Major Professor

Daping Fan, Committee Member

Claudia Grillo, Committee Member

Michael A. Matthews, Committee Member

Wenbin Tan, Committee Member

Cheryl L. Addy, Interim Vice Provost and Dean of the Graduate School

DEDICATION

To my parents, whose love, support, and sacrifice made this achievement possible.

ACKNOWLEDGEMENTS

First and foremost, thanks be to God, who I have called on for support more times than I can count throughout this process. Thank you to my parents, Greg and Jane, and my brothers, David and Andrew, for their unconditional love and support. Without them, this would have been an impossible endeavor. Thanks also to my Grandaddy, Dr. George F. Stroope, who has inspired me from the time I was a little girl. I am deeply appreciative of the encouragement I have received from many other loved ones and friends, who I consider to be family.

On a professional level, I'd first like to thank my mentor, Dr. Wayne Carver, whose instruction, and patience have been invaluable throughout my journey. It should be noted that he took a chance on me as a student who wasn't initially so sure about research, and I am immensely grateful. Thanks also to Drs. Daping Fan, Claudia Grillo, Mike Matthews, and Wenbin Tan for serving on my committee and for their support, kindness, and valuable feedback. I'd also like to thank our laboratory technician and extraordinaire, Charity Fix, for her patience, guidance, support, humor, and dedication to my personal and professional success. She has become a great friend, and any future success I might have will be, in part, due to her mentorship. I cannot thank her enough. I would also like to acknowledge our Biomedical Sciences Student Services Program Coordinator, Joann Nagy; her friendliness and dedication to the graduate program has not gone unnoticed.

I received assistance from a handful of other students and lab groups at various times that deserve recognition. First, thanks to undergraduate students Ethan Fix, Katie Derr, and Sarah Stofik, who worked with me at different times over the last several years. Thanks also to Colton Kostelnik for harvesting tissue weekly and the IRF staff, especially Lorain Junor and Ryan Ball, for their assistance with experiments and various equipment outside of my lab.

I would also like to thank the many friends who made the last six years a lot more fun and meaningful. I had a great time being a part of various student organizations on campus, a member of the Pi Beta Phi Columbia Alumnae Club, and being a parishioner at St. Joseph Catholic Church. I'd also like to thank my girlfriends from Females in Action (FiA) who provided many laughs and encouragement when this work seemed overwhelming, especially over the last year. All these friendships and experiences have contributed in some small way to the completion of this mountain of work, and I am enormously thankful.

ABSTRACT

In 2017, over 3.5 million peripheral vascular surgeries were performed worldwide with over 400,000 vascular repair or replacement surgeries being performed in the United States each year alone. As the number of vascular repair surgeries, including both coronary and peripheral bypass grafting procedures, continues to increase each year, these statistics indicate an urgent need for more effective and readily available replacement materials. Regenerative medicine and tissue engineering (TE) approaches, including the design, fabrication, and validation of suitable biomaterials *in vitro* that direct the repair and regeneration of damaged tissues, have been proposed to alleviate this problem. While advanced biomaterials have made significant headway in the engineering of complex replacement tissue scaffolds, several hurdles remain before this technology reaches its full potential. In the application of tissue-engineered blood vessels as a platform for coronary and peripheral artery bypass grafting procedures these hurdles include increased thrombogenicity, poor recellularization, and mechanical mismatch, ultimately leading to decreased patency of the vessel. In addressing these hurdles, decellularized blood vessels have gained substantial popularity as a platform for TE vascular grafts; however, this remains challenging, as there is a pressing need to optimize decellularization protocols for small-diameter blood vessels to produce vascular scaffolds with properties mirroring that of native tissue.

One method for producing effectively decellularized TE scaffolds is chemical decellularization, which has been successfully achieved through the use of the anionic

detergents sodium dodecyl sulfate (SDS) and sodium deoxycholate (SDC). These homogeneously disrupting surfactants solubilize cell membranes and can be very effective decellularization agents; however, exposure at high concentrations or for long durations can damage the extracellular matrix and can be cytotoxic. We initially investigated the differential response of varying 0%−6% SDS and SDC anionic detergent concentrations after 24 and 72 h in the presence of DNase using biochemical, histological, and biaxial mechanical analyses to optimize the decellularization process for xenogeneic vascular tissue sources, specifically the porcine internal thoracic artery (ITA). Detergent concentrations greater than 1% were successful at removing cytoplasmic and cell surface proteins, but not DNA content after 24 h. A progressive increase in porosity and decrease in glycosaminoglycan (GAG) content was observed with increasing detergent concentration. Prolonged treatment significantly improved decellularization by reducing DNA content to trace amounts after 72 h, but also reduced laminin content and influenced the vessel's mechanical behavior. Collectively, DNase with 1% detergent for 72 h provided an effective and efficient decellularization strategy to be employed in the preparation of porcine ITAs as bypass graft scaffolding materials. Yet this was at the cost of altered mechanical properties and laminin retention.

Supercritical carbon dioxide ($scCO_2$) has received attention as an alternative strategy for tissue decellularization to potentially alleviate the problems associated with the traditional chemical and physical decellularization methods; however, this strategy has been evaluated in limited tissue types and methods are far from optimized with this approach. We turned our focus to developing a novel optimized $scCO_2$ protocol that would lead to a more time-efficient decellularization method and would yield a small-

diameter vascular scaffold with enhanced structural, biomechanical, and biochemical properties compared to the decellularized scaffold products generated with chemical methods alone. The experimental conditions utilized in this study, 0.5% SDS for 2 and 24 h, were established to evaluate the effects of $scCO_2$, DNase, and SDS alone or in combination on porcine ITA decellularization. Both the 2 h and 24 h SDS/$scCO_2$ hybrid treatments removed sufficient DNA content, which allowed us to selectively continue our experiments using the 2 h SDS/$scCO_2$ hybrid treatment as to prevent the tissue from being exposed to detergent for longer than is necessary to achieve adequate decellularization. 2 h of 0.5% SDS treatment plus $scCO_2$ was successful at removing cytoplasmic and cell surface proteins and DNA content. There was not a significant difference in sGAG concentration across any of the conditions analyzed, yet an increase in the concentration was observed in the samples treated with detergent alone and with detergent plus $scCO_2$. However, tissue porosity appeared to increase between detergent alone and detergent plus $scCO_2$-treated samples, but this was not directly quantified. Collectively, these findings suggest that very low detergent concentrations coupled with $scCO_2$ treatment can be used in future decellularization strategies, but at the cost of some laminin retention. However, further study is required to determine the possibilities and limitations of this method, including bioactivity studies, testing $scCO_2$-generated scaffolds as replacement material in animal models, and assessing biochemical modification of the scaffolds.

This dissertation confirms the use of a hybrid protocol including detergent plus $scCO_2$ as: (1) a method of decellularization that can be optimized for the decellularization of porcine ITAs and, (2) a more-efficient decellularization method that yields a small-

diameter vascular scaffold with similar structural and biochemical properties compared to those of the enzyme-detergent methods also presented in this work. The use of $scCO_2$ for decellularization can be expanded to additional tissues once the SDS/$scCO_2$ hybrid method is better understood in porcine ITAs. Additionally, it is possible that $scCO_2$ could be used to simultaneously decellularize and sterilize tissues in the future. These studies provide insight into the effects of anionic detergent concentration and incubation time on porcine ITA decellularization and demonstrate an optimized decellularization procedure using a $scCO_2$-based hybrid treatment. These are significant contributions to the field of tissue engineering, especially involving the potential development of more appropriate replacement materials for both coronary and peripheral bypass grafting procedures.

TABLE OF CONTENTS

Dedication iii

Acknowledgements iv

Abstract vi

List of Tables xii

List of Figures xiii

List of Symbols xv

List of Abbreviations xvi

Chapter 1: Introduction 1

1.1 Decellularization 4

1.2 Dissertation Objectives 15

Chapter 2: Decellularization of Porcine Internal Thoracic Arteries Using Anionic Detergents 19

2.1 Introduction 19

2.2 Materials and Methods 22

2.3 Results and Discussion 29

2.4 Conclusions 35

Chapter 3: Decellularization of Porcine Internal Thoracic Arteries Using Supercritical CO_2 48

3.1 Introduction 48

3.2 Materials and Methods 51

3.3 Results and Discussion 59

3.4 Conclusions....70

Chapter 4: Final Conclusions and Future Directions....85

References....90

LIST OF TABLES

Table 2.1 List of Detergent Decellularization Treatments.....37

Table 3.1 List of Hybrid Detergent-scCO$_2$ Treatments.....72

LIST OF FIGURES

Figure 1.1 Schematic of Organ and Tissue Decellularization Approaches 17

Figure 1.2 Carbon Dioxide Phase Diagram 18

Figure 2.1 DAPI Stain Following Anionic Detergent Treatment 38

Figure 2.2 Quantification of DNA Content From PicoGreen Assays (Detergent) 39

Figure 2.3 Western Blot Analysis of Representative Proteins (Detergent) 40

Figure 2.4 Quantification of DNA Content From PicoGreen Assays (+/- DNase) 41

Figure 2.5 Representative Scanning Electron Microscopic Images (Detergent) 42

Figure 2.6 Quantification of Hydroxyproline Concentrations (Detergent) 43

Figure 2.7 Quantitative Analysis of Elastic Fibers (Detergent) 44

Figure 2.8 Analysis of Dimethylmethylene Blue Concentrations (Detergent) 45

Figure 2.9 Biaxial Mechanical Data for Detergent Decellularized Groups 46

Figure 2.10 Biaxial Mechanical Data at Common Loading Conditions 47

Figure 3.1 Supercritical CO_2 Decellularization Schematic 73

Figure 3.2 DAPI Stain Following 24 h SDS/scCO_2 Treatment 74

Figure 3.3 DAPI Stain Following 2 h SDS/scCO_2 Hybrid Treatment 75

Figure 3.4 Quantification of DNA Content From PicoGreen Assays (Hybrid) 76

Figure 3.5 Western Blot Analysis of Representative Proteins (Hybrid) 77

Figure 3.6 Representative Scanning Electron Microscopic Images (Hybrid) 78

Figure 3.7 Quantification of Hydroxyproline Concentrations (Hybrid) 79

Figure 3.8 Quantitative Analysis of Elastic Fibers (Hybrid) 80

Figure 3.9 Analysis of Dimethylmethylene Blue Concentrations (Hybrid) 81

Figure 3.10 Quantification of Residual SDS (Hybrid) 82

Figure 3.11 Biaxial Mechanical Data of 2 h SDS/scCO$_2$ (0-200 mmHg) 83

Figure 3.12 Biaxial Mechanical Data of 2 h SDS/scCO$_2$ (Common Loading Cond.).....84

LIST OF SYMBOLS

n	n-value for statistical tests
p	p-value for statistical tests indicating statistical significance
P	Pressure
P_c	Critical Pressure
T	Temperature
T_c	Critical Temperature

LIST OF ABBREVIATIONS

BCA ..... Bicinchoninic Acid

CABG ..... Coronary Artery Bypass Graft

CO_2 ..... Carbon Dioxide

DAPI ..... 4’,6-Diamidino-2-Phenylindole

dECM ..... Decellularized Extracellular Matrix

DMMB ..... Dimethylmethylene Blue

DNA ..... Deoxyribonucleic Acid

ECM ..... Extracellular Matrix

ePTFE ..... Expanded Polytetrafluoroethylene

H&E ..... Hematoxylin and Eosin

HHP ..... High Hydrostatic Pressure

HMDS ..... Hexamethyldisilazane

ITA ..... Internal Thoracic Artery

PBS ..... Phosphate-Buffered Saline

PSR ..... Picrosirius Red

RPM ..... Revolutions Per Minute

$scCO_2$ ..... Supercritical Carbon Dioxide

SCF ..... Supercritical Fluid

SDC ..... Sodium Deoxycholate

SDS ..... Sodium Dodecyl Sulfate

SDS-PAGE ..... Sodium Dodecyl Sulfate Polyacrylamide Gel Electrophoresis

SEM ..... Scanning Electron Microscopy

s-GAG ..... Sulfated-Glycosaminoglycan

TE ..... Tissue Engineering

VVG ..... Verhoeff-Van Gieson

CHAPTER 1

INTRODUCTION

In 2017, over 3.5 million peripheral vascular surgeries were performed worldwide with over 600,000 vascular repair or replacement surgeries being performed in the United States each year alone (Go et al., 2013). Coronary artery bypass is the most common type of heart surgery with more than 400,000 procedures performed in the United States annually, according to statistics from the American Heart Association published in *Circulation* (Thom et al., 2006). As the number of vascular repair surgeries, including both coronary and peripheral bypass grafting procedures, continues to increase each year, these statistics indicate an urgent need for more effective and readily available replacement materials.

A variety of approaches are used to generate small-diameter replacement vessels including the use of the patient's own vessels (autograft), utilization of donor grafts from a different individual (allograft), or utilization of engineered grafts composed of biological or synthetic materials or a hybrid of these. Peripheral artery and coronary artery bypass grafts (CABG) may utilize autologous or synthetic vessels. Yet when targeting small-diameter vessel replacements (<6 mm internal diameter), autologous grafts harvested from the patient currently offer superior outcomes when compared to synthetic materials (Bergmeister et al., 2013; Seifu et al., 2013). The most used autografts are saphenous veins, radial arteries, or internal thoracic arteries, as they provide natural biocompatibility, are non-thrombogenic, and possess appropriate mechanical properties

(Seifu et al., 2013). Among these, the saphenous vein is the most widely used graft in small-diameter vascular graft replacements. This dependence on autologous grafts is due to the lack of small-diameter synthetic graft alternatives that are clinically viable (Wang et al., 2007; Desai et al., 2011), with synthetic grafts experiencing patency rates >60% within in the first year after implantation compared to that of saphenous vein grafts (90% after the 1st year of implantation) (Chard et al., 1987; Shah et al., 2005; Hadinata et al., 2009). However, significant downsides also accompany the use of autologous vessels. It is estimated that >30% of patients with cardiovascular disease (CVD) lack suitable vessels (Matsuzaki et al., 2019). Repetition of the surgery is also limited by availability of the vessel if used previously (Seifu et al., 2013). Moreover, autografts are subject to pathological remodeling called vein graft disease when used as vascular grafting material (Klinkert at al., 2004; Conte MS, 2013). Saphenous vein graft (SVG) disease is characterized by thrombosis, intimal hyperplasia, and atherosclerosis, and endothelial damage has been shown to be the major underlying pathophysiology of SVG disease (Kim et al., 2013). Despite surgical advances, approximately one-half of vein grafts fail by 5 to 10 years post-surgery and this failure is associated with worse clinical outcomes (Parang et al., 2009; Hall et al., 2019). Attempts have also been made to establish cryopreserved allograft veins (CAVs), dating back as far as the 1980s, as bypass substitutes. Such allografts have been used in patients without sufficient autologous graft material; however, given the poor early and late patency rates, CAVs have not become widely accepted as bypass graft alternatives (Conte MS, 1998; Lamm et al., 2001).

Currently, synthetic grafts and patches composed of polymers such as polyethylene terephthalate (PET, Dacron) and expanded polytetrafluoroethylene (ePTFE,

Gore-Tex) exhibit lower patency than autologous grafts, but have been implanted in large numbers of patients over the last several decades and are relatively effective for the repair of large diameter blood vessels (>8 mm diameter) such as the aorta (Hiob et al., 2017). However, these are limited in use as grafting material for small-diameter vessels (1-6 mm) because they are susceptible to occlusion. Furthermore, the blood flow in small-diameter vascular grafts, higher thrombogenicity of the graft material, and the poor homogeneity in the compliance of the native vessel and the graft are all factors that contribute to the low patency of synthetic grafts between 1-6 mm (Hoenig et al., 2005; Kannan et al., 2005; Desai et al., 2011; McBane et al., 2012; Seifu et al., 2013). Because of complications with these approaches, there remains an urgent need to develop effective tissue-engineered substitutes for cardiovascular and other tissues (Gershlak et al., 2017).

One relatively novel way to address this obstacle is through the production of acellular or decellularized extracellular matrix (dECM) scaffolds from xenogeneic vascular tissues by way of tissue engineering (TE), introduced in Figure 1.1. dECM scaffolds, biomaterials formed by human or animal organs/tissues with the removal of immunogenic cellular components via decellularization technologies, have come center stage. These scaffolds mainly consist of extracellular matrix (ECM), including ECM proteins such as collagen, elastin, laminin, and fibronectin, and maintain their biological and mechanical performance after decellularization. This is important as maintaining a biomimetic structure is critical for subsequent cell-seeding and reimplantation (Ahmed et al., 2021). Therefore, these recellularized dECMs could be used as potentially functional

constructs as a regenerative medicine strategy for the replacement of damaged tissues or tissue repopulation.

While the use of TE to produce dECM scaffolds works well theoretically, a number of challenges have prevented its successful use in widespread clinical practice. Effective dECM scaffolds must preserve the original architecture and composition and biochemical and mechanical properties of the native ECM. Some of the criteria for successful dECM utilization include (Zhang et al., 2021):

- Suitable morphology for tissue-specific application
- Maintaining structural integrity to withstand mechanical forces
- High biocompatibility/low immunogenicity to prevent host immune response
- Bioactive and able to promote constructive remodeling
- Devoid of any residual cytotoxic agents

1.1 Decellularization

Xenogeneic tissues contain non-autologous or foreign cells which must be removed prior to reseeding the scaffold to prevent any unwanted immune response post-implantation (Wiles et al., 2016). Decellularization is the process used to isolate the ECM of a tissue from its inhabiting cells, leaving behind an ECM scaffold of the original tissue. As indicated above, the ultimate goal of decellularization is to rid the ECM of native cells and genetic materials such as DNA while maintaining its structural, biochemical, and biomechanical properties (Gilpin et al., 2017; Nakamura et al., 2017).

Because tissues vary widely, the most effective agents for decellularization of each tissue and organ will depend on a host of factors, including thickness, ECM composition, cell type, cell density, and lipid content (Crapo et al., 2011). It is important

to point out that all known decellularization processes will alter the ECM composition and microstructure to some degree; however, minimization of these undesirable effects rather than total avoidance is the overall objective. Commonly used decellularization methods will be discussed in a subsequent section of this chapter.

To date, there is no universal or widely agreed upon protocol for decellularization. The decellularization process itself is a delicate balance, since harsh protocols run the risk of degrading ECM structure and compromising the mechanical integrity of the tissue, while mild protocols fail to remove all foreign cellular material that might induce an unwanted immune response in the patient (Mikos et al. 1998). Moreover, it is accepted in the field that no one decellularization method can remove all cellular content entirely, and that all methods of decellularization disrupt the structure and composition of the ECM to some degree (Crapo et al., 2011; Keane et al., 2015). Thus, the key and challenge then in creating a standard decellularization protocol is to find the balance between sufficient removal of cellular content as to prevent an immune response while preserving ECM structures to promote constructive remodeling (Badylak et al., 2012). Both criteria are essential for the development and success of using recellularized scaffolds for clinical applications, which means these criteria should be used to determine the effectiveness of any given decellularization procedure. As previously discussed, there is still no universal consensus or gold-standard criteria for adequate decellularization; however, Crapo *et al.* proposed standard metrics to address this need. This 2011 review suggested the following criteria to characterize fully decellularized materials (Crapo et al., 2011):

1. Less than 50 ng of double-stranded DNA per mg ECM dry weight
2. DNA fragment length of less than 200 base pairs

3. Lack of visible nuclear material in tissue sections stained with DAPI or hematoxylin and eosin (H&E)

While this remains the suggested standard, it has yet to become widely accepted as the universal standard. There are also no standard criteria for ECM preservation following decellularization; however, research groups typically assess ECM protein composition, biomechanical properties, and scaffold structure and compare these properties to those of native tissue.

1.1.1 Decellularized ECM Scaffolds: Chemical, Physical, and Enzymatic Methods

Decellularization has been performed on almost every tissue in the body, including adipose tissue (Flynn et al., 2010), blood vessels (Kostelnik et al., 2021), bone (Tran et al., 2021), cornea (Mahdavi et al., 2020), esophagus (Mallis et al., 2019), heart (Ott et al., 2008), intestine (Kitano et al., 2017), kidney (Ross et al., 2009), liver (Baptista et al., 2011), lung (Ott et al., 2010), nerve (Gregory et al., 2022), pancreas (Hashemi et al., 2018), skin (Wolf et al., 2012), thymus (Campinoti et al., 2020), and others. The source of these decellularized tissues is typically of mammalian origin, including porcine, bovine, or murine (Keane et al., 2015). While there are a host of different decellularization methods and agents, most protocols describe sequential and combinatorial use of a variety of physical, chemical, and enzymatic techniques to achieve tissue-specific decellularization.

Generally, chemical and enzymatic techniques are primarily responsible for successful decellularization in most protocols (Mendibil et al., 2020). Chemical treatments involve the use of chemical detergents (surfactants) to solubilize cell membranes. Of the many types of detergents, the two most commonly used are Triton

X-100 and sodium dodecyl sulfate (SDS). Triton-X is a non-ionic surfactant that targets the lipid–lipid protein interactions, but leaves this interaction intact (Cartmell et al., 2000; Woods et al., 2005). This agent is most effective in tissues in which the key component of the ECM is primarily proteins. While Triton-X effectively eliminates cells from most tissues, excluding those that are denser, its use is typically avoided for tissues in which glycosaminoglycans (GAGs) are the primary component (Liao et al., 2008; Mendibil et al., 2020). Their maintenance is important because GAGs are polysaccharide ECM components that play a role in the creation of conducive microenvironments for a number of essential cellular activities and are essential in defining tissue architecture and mechanical properties of vascular tissue (Bruyneel et al., 2017). Conversely, SDS is an ionic surfactant that solubilizes both external and nuclear membranes and disrupts covalent protein–protein bonds. While SDS is very efficient in removing nuclear and cytoplasmic content, it tends to denature proteins and can alter the native structure of the matrix (Elder et al., 2010). Cytotoxicity due to residual SDS is another concern when using this detergent for decellularization (Gilbert et al., 2006). The effects of SDS and sodium deoxycholate (SDC), another ionic detergent, are concentration and time-dependent and thus their inclusion in decellularization protocols should be carefully titrated.

While not as common, other detergents are useful for tissue-specific decellularization. CHAPS is a zwitterionic surfactant meaning it shares properties with both ionic and nonionic detergents (Moffat et al., 2022). CHAPS disrupts lipid–protein and lipid–lipid interactions; however, its reduced permeating qualities limit its ability to remove nuclear DNA. Acids and bases are another type of chemical decellularization

agent; however, they are rarely used due to their harshness toward the proteins of the matrix.

Enzymes, including proteases and nucleases, are also used in decellularization protocols, mainly because of their substrate specificities; however, exposure to some proteases at high concentrations or for prolonged periods can damage the collagenous matrix of tissues (Brown et al., 2011; Meyer et al., 2019). Trypsin, a serine protease that cleaves peptide bonds on the C-side of arginine and lysine, is the most commonly used enzyme in decellularization protocols and is typically combined with ethylenediaminetetraacetic acid (EDTA), a chelating agent, that breaks cell–matrix interactions (McFetridge et al., 2004; Chen 2013). However, ECM proteins such as collagen have limited resistance to trypsin cleavage (Waldrop et al., 1980), therefore tissue exposure to trypsin should be used with caution. Prolonged exposure to trypsin can disrupt ECM ultrastructure, and remove ECM constituents including collagen, laminin, fibronectin, elastin, and glycosaminoglycans (GAGs); yet there is a slower removal of GAGs compared to detergents (Crapo et al., 2011). The use of enzymatic treatment with endonucleases (e.g., DNase) following detergent treatment is also common to cleave nucleotide bonds and achieve more complete decellularization than with SDS alone (Simsa et al., 2018).

Among physical manipulations to decellularize tissues, freeze-thaw cycles have been widely used either alone or in combination with chemical methods. While producing some disruptions in the tissue architecture, freeze-thaw cycles do not appear to significantly alter the biomechanical properties of the ECM (Cebotari et al., 2010; Nonaka et al., 2014). Pressure gradients, described by Keane *et al.*, or agitation are other

physical methods often used with chemically induced decellularization primarily to enhance penetration of the chemical into the tissues (Keane et al., 2015). A common physical decellularization approach is immersion of tissues in decellularization agents while being subjected to agitation (Crapo et al., 2011). Agitation in conjunction with immersion leads to cell lysis, yet it is mostly used with chemical agents to enhance the exposure of the ECM to the detergents and to strengthen the decellularization process (Neishabouri et al., 2022). Immersion and agitation methods of tissue decellularization have been performed on a number of tissues, including blood vessels (Lehr et al., 2010; Kostelnik et al., 2021), cartilage (Elder et al., 2010), dermis (Belviso et al., 2020), esophagus (Ozeki et al., 2006), heart valves (Faggioli et al., 2022), urinary bladder (Yang et al., 2010), among others. The duration of a protocol using immersion and agitation is dependent upon the thickness and density of the tissue, the detergent used, and agitation intensity (Crapo et al., 2011; Keane et al., 2015). For example, thin tissues such as the urinary bladder or small intestine have been decellularized following relatively short exposure to peracetic acid with agitation. For these and narrow pieces of other tissues, the DNA removal and loss of ECM components are a function of agitation speed during decellularization (Crapo et al., 2011). More dense tissues such as dermis and trachea require much longer exposure (days to months) to combinations of detergents, enzymes, and alcohols. Like agitation, sonication is also used to lyse cells or dislodge them from the ECM (Lin et al., 2021). It has been demonstrated that direct or indirect sonication increases agent penetration into the scaffold, hence enhancing chemical decellularization while causing less damage to the structural integrity of the ECM (Forouzesh et al., 2019). However, aggressive agitation or sonication can disrupt the ECM.

Approaches to decellularize whole organs have been developed incorporating traditional decellularization techniques, but, unlike smaller and more simply structured tissues, whole organs require more sophisticated processing due to their thicker, and more complex architecture. To overcome this challenge, vascular perfusion decellularization has been applied to these whole organs and has largely preserved the architecture of the ECM and the organ as a whole (Crapo et al., 2011; Guyette et al., 2014). Perfusion through the vasculature is an efficient method of delivering decellularizing agents through the tissues, and it has been shown to homogenously decellularize tissues (Ott et al., 2008; Baptista et al., 2011).

Another critical aspect of the tissue-engineering process is recellularization. Recellularization is the repopulation of acellular ECM scaffolds of tissues or organs with tissue-specific cell types or stem cells (e.g., induced pluripotent stem cells (iPSCs), embryonic stem cells) aiming to reconstruct the microstructure of the tissue and thus recreate the tissue-specific function. The cells used for repopulation need guidance for their rearrangement and maturation, a task that is better performed by the ECM and its residual components (Hillebrandt et al., 2019). Preserving tissue-specific ECM components such as growth factors and structural proteins during decellularization is essential, as these help to facilitate an optimal recellularization process (Park et al., 2016). Recellularization is typically performed using two different techniques. The first technique, which is dependent on cell type, involves recellularization via the vascular network or another hollow structure (e.g., airway, intestinal lumen, or ureter). Secondly, it is also possible to recellularize via direct cellular injection into the parenchyma. For successful recellularization, the repopulation of the vascular ECM network with

endothelial cells is required to prevent thrombogenicity and possible subsequent loss of the tissue graft. Whole-organ recellularization requires an environment that mimics the physiological conditions of the specific organ (Hillebrandt et al., 2019). To address this, *ex vivo* bioreactor systems have been commonly employed in tissue recellularization studies (Adil et al., 2022), as the design of these systems is often tailored to mimic *in vivo* physiological conditions. Key features for bioreactor systems include the ability to tailor flow rates, ability to monitor cell culture condition parameters (e.g., pH, oxygen, metabolites), leak-proof and sterilizable components, easy assembly, and ease in inserting/retrieving scaffolds (Ahmed et al., 2019). These features are particularly important because recellularization heavily relies on the cell culture conditions to support cell survival and growth within scaffolds with considerations required for different cell types, cell medium composition, respective growth factors and supplements, and cell seeding densities (Mohammadi et al., 2021). It is also advantageous to tailor recellularization strategies to control cell proliferation, differentiation, and subsequent maturation of cells in regenerating tissues. Therefore, recellularization and regeneration of tissues is interdependent on cell culture and maturation strategies to promote tissue functionalization (Adil et al., 2022).

1.1.2 Decellularized ECM Scaffolds: Supercritical Carbon Dioxide ($scCO_2$)

An optimal decellularization method using any of the techniques cited above has yet to be demonstrated, and several hurdles remain to fully realize the potential of these more conventional techniques. Chemical decellularization techniques are very time consuming, typically requiring several days or weeks to complete. Additionally, residual cytotoxic detergents remain within scaffolds even after thorough rinsing with most

chemical detergent treatments (Keane et al., 2012; Fernandez-Perez et al., 2019). As previously discussed, detergents can also have deleterious effects on the native ECM architecture (Faulk et al., 2014). Because of these obstacles, there remains a need for novel decellularization practices.

One method of processing biomaterials that has continued to be of interest over the last 20 to 30 years is the use of supercritical fluids (SCFs). A supercritical fluid refers to a substance above its critical temperature (T_c) and critical pressure (P_c). Together these are known as the critical point (T_c, P_c). Supercritical fluids are effective solvents because they have a unique combination of properties: densities on the order of liquids but diffusivities and viscosities on the order of gases (Carlès et al., 2010). Along with having minimal surface tension, these properties together allow SCFs to penetrate pores and surface openings without damaging them (McHugh et al., 1994). The SCF outgasses upon depressurization, which means the SCF that was dissolved, trapped, or absorbed in the material is released. Unlike previously described conventional techniques, this prevents concerns with any residual cytotoxicity.

Supercritical carbon dioxide ($scCO_2$) is the most commonly used SCF. $scCO_2$ is carbon dioxide that has been highly compressed and heated past its critical temperature. It is chemically inert, relatively non-toxic, and non-flammable, which are all significant safety and environmental advantages that make it the most preferred supercritical fluid (Beckman, 2004). $scCO_2$ also has relatively low critical conditions (31°C; 7.40 MPa) making it well-suited for biomedical applications including the fabrication of tissue engineering scaffolds (Davies et al., 2008; Sherifi et al., 2020; Rabbani et al., 2021), the sterilization of natural and synthetic biomaterials (Ellis et al., 2010; Garcia-Gonzalez et

al., 2015), and the production of nanocomposites (Salarian et al., 2014; Moghadas et al., 2019) among other applications.

To better understand the effects of temperature and pressure on $scCO_2$, a temperature-pressure diagram for a pure substance, such as CO_2 is shown in Figure 1.2. The diagram consists of the one-phase regions (solid, liquid, and vapor) and two-phase curves, indicated in Figure 1.2, where thermodynamic equilibrium exists between the two phases. There are also two temperature-pressure coordinate points of interest, the triple point and the critical point. The triple point is the point at which the solid, liquid, and vapor phases exist in three-phase equilibrium. However, the most important point of interest for this work is the critical point. As this point is approached, the liquid and vapor phases advance toward equal densities and the phase boundary disappears. CO_2 enters the supercritical phase, also shown in Figure 1.2, once the temperature and pressure of its critical point are exceeded (White et al., 2021).

To address the deficiencies of more traditional chemical and physical decellularization methods, $scCO_2$ has gained popularity as a novel and more innovative approach (Guler et al., 2017; Casali et al., 2018; Harris et al., 2021). High hydrostatic pressure (HHP), a form of physical treatment, followed by extended washing has been used to decellularize aortic tissue (Funamoto et al., 2010), which previously suggested potential for $scCO_2$ in decellularization, as its pressure is far lower than that of HHP. Prior to the Matthews group in 2018 (Casali et al., 2018), decellularization using $scCO_2$ had been completely unexplored except for the Sawada group in 2008 (Sawada et al., 2008). While Sawada *et al.* reported 100% removal of DNA using $scCO_2$ and an ethanol additive to decellularize porcine aortas, they also described significant dehydration of the

matrix and loss of mechanical strength (Sawada et al., 2008). Years later, however, Casali *et al.* proposed and successfully executed a decellularization method using $scCO_2$ that preserved the matrix hydration state and mechanical properties by presaturating the $scCO_2$ with water (Casali et al., 2018). They reported incomplete decellularization with $scCO_2$ alone and instead developed a novel hybrid method that combined brief (48 h) exposure of tissue to aqueous detergent, followed by treatment with $scCO_2$ for 1 h. This hybrid method fully decellularized the tissue, which was confirmed by histology and DNA quantification. However, the parameters of their hybrid method (e.g., SDS concentration and treatment time, $scCO_2$ treatment time, and depressurization rate) were not optimized.

Since 2018, SCF-based technologies have been increasingly utilized for tissue engineering and other biomedical applications. In particular, SCF-based decellularization protocols are being more frequently employed. For example, Topuz *et al.* has studied the potential of $scCO_2$ for the decellularization of myocardium, optic nerve, and corneal tissues to produce naturally-derived scaffolds for implantation (Topuz et al., 2020). For the optic nerve, histological analysis revealed that nuclei were significantly removed, and DNA quantification revealed that residual DNA was less than 50 ng dsDNA per mg ECM dry weight. While the processing also preserved the integrity of the nerve ECM, it caused a considerable reduction in the size of treated samples (Topuz et al., 2020). More recently, Duarte *et al.* experimented with the use of TnBP, a solvent previously used to decellularize tendons, as a co-solvent for $scCO_2$-assisted decellularization of trabecular bone (Duarte et al., 2020). While various protocols led to a decrease in DNA content,

depending on TnBP concentration and $scCO_2$ run-time, no protocol achieved less than 50 ng per mg ECM dry weight, and nuclear material remained visible after H&E staining.

Because of the need for a more benign alternative than harsh chemical treatments, there are many more groups interested in using $scCO_2$-assisted decellularization than there were in 2018. Yet some critical areas where research is still required in the use of $scCO_2$ decellularization is in fully understanding how processing protocols impact morphology, mechanical performance, degradation profile, quantification of GAG content, and other relevant biological parameters (Duarte et al., 2021).

1.2 Dissertation Objectives

The utilization of dECM scaffolds for small-diameter blood vessel replacement have not yet reached their full potential. This is due to less-than-optimal decellularization and biochemical modification processes that lead to inferior biomechanical properties as well as poor cell repopulation and differentiation within the scaffold. The overarching objective of this dissertation is to focus on the optimization of the decellularization process of xenogeneic vascular tissue to promote effective retention of ECM components and biomechanical integrity of the resulting scaffolds. This objective was accomplished by using anionic detergents and $scCO_2$ to treat porcine internal thoracic arteries. The specific aims of this work are: (1) evaluate the effects of anionic detergent concentration and incubation time on porcine internal thoracic artery (ITA) decellularization and, (2) optimization of the decellularization procedure of porcine ITA tissue using $scCO_2$-based hybrid treatment to generate a standard and more time-efficient procedure than detergent-only methods. Both specific aims were focused on determining the relative effects of key process parameters on cell removal and scaffold properties.

While much work has been done on fabrication of TE dECM scaffolds using chemical and physical parameters, there is still no methodological gold standard of decellularization, which is dependent on numerous factors. Likewise, the fabrication of TE scaffolds using $scCO_2$ is becoming more prominent; however, there are still many questions to be answered. The findings of this dissertation will be used to optimize the decellularization process of xenogeneic tissue and further elucidate how detergent-enzyme processes and $scCO_2$ interacts with scaffold properties. This knowledge may contribute to the development of an acellular scaffold that can be used to investigate tissue remodeling and can be leveraged for future clinical application.

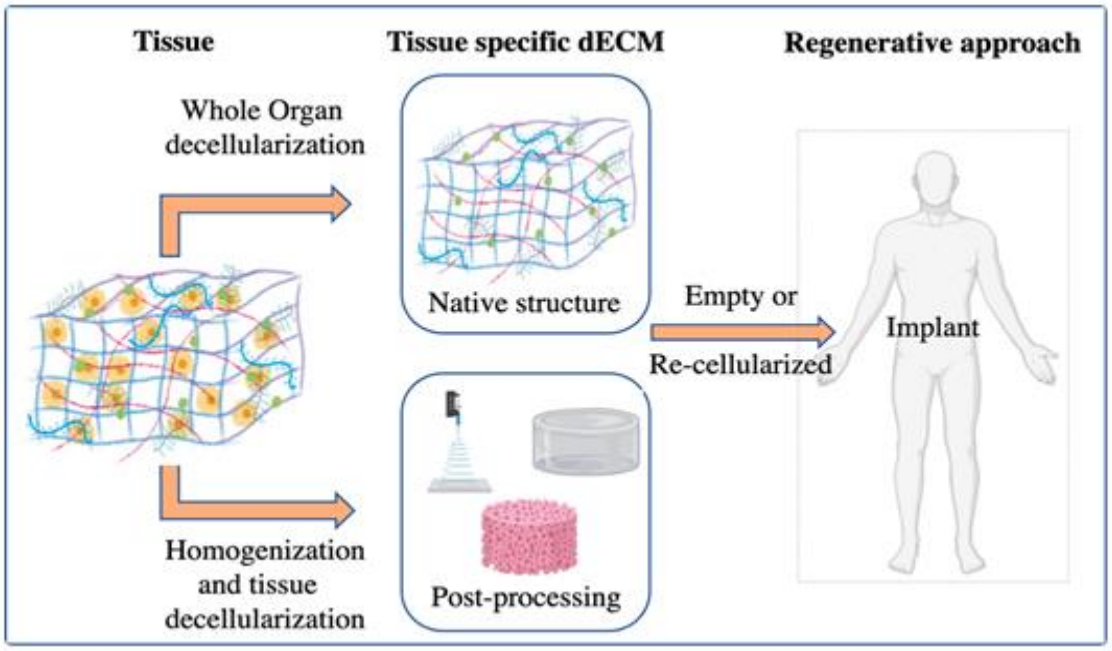

Figure 1.1 – Schematic of Organ and Tissue Decellularization Approaches (Mendibil et al., 2020).

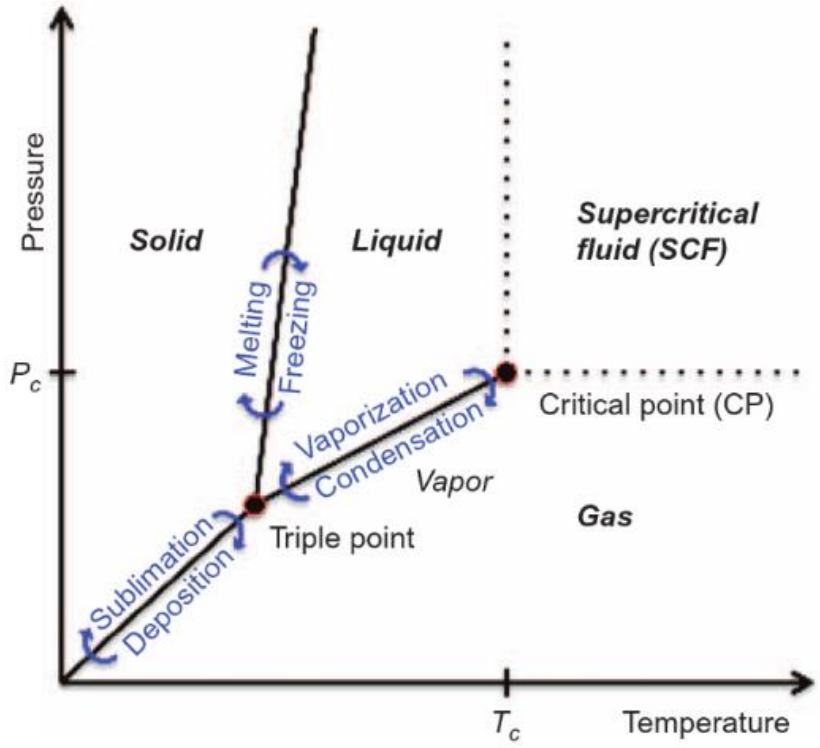

Figure 1.2 – Carbon Dioxide Phase Diagram (Cunico et al., 2017).

CHAPTER 2

DECELLULARIZATION OF PORCINE INTERNAL THORACIC ARTERIES USING ANIONIC DETERGENTS

2.1 Introduction

A major challenge confronting the field of regenerative medicine and tissue engineering is the design, fabrication, and validation of scaffolds that direct the repair and regeneration of damaged tissues (Ikada et al., 2006; Celikkin et al., 2017). Advanced biomaterials including hydrogels, membranes, micro/nanofibers, and micro/nanoparticles have emerged as innovative platforms for tissue engineering purposes (Cross et al., 2016; Mehrali et al., 2017; Vedadghavami et al., 2017). New generation biomaterials and novel technologies are making substantial headway in the engineering of complex tissue scaffolds. This is due in part to the ability to modulate the composition and microarchitecture of these materials to improve biocompatibility, promote desirable cellular events, and optimize degradation kinetics and mechanical properties. Advances in biomaterials are making the engineering of replacement tissues a reality; however, several hurdles remain before this technology reaches its full potential. These hurdles are particularly evident in the application of tissue-engineered blood vessels as a platform for coronary and peripheral bypass grafting procedures. With approximately 400,000 bypass surgeries occurring annually in the United States alone, there is a pressing need to optimize replacement blood vessels for grafting surgeries (Go et al., 2014; Li et al; 2014).

Autografts are the preferred choice in small-diameter vascular bypass procedures due to their biocompatibility and lack of thrombogenicity. However, they are inherently limited in use for bypass procedures due to the number of bypasses a patient may require and any chronic pathological conditions that impact tissue patency such as atherosclerosis or diabetes. Prosthetic grafts or patches (e.g., Dacron or expanded PTFE) have been implanted in large numbers of patients over the past several decades and these are relatively effective for the repair of large arteries such as the aorta. However, these prosthetic grafts are limited for use in bypass procedures because increased rates of infection and thrombotic events have been detected when used as small-diameter blood vessel replacements (Krishnan S et al., 2006; Bachleda et al., 2012). Decellularized blood vessels have gained popularity as a biomimetic scaffold by harnessing innate tissue-specific properties to direct cellular functions including differentiation and proliferation while inducing a minimal immune response (Gilbert et al., 2006; Tapias et al., 2014; Gilpin et al., 2017). Such scaffolds can be created from human or animal tissues and are a low-cost and readily available platform for tissue engineering. In their native form, decellularized scaffolds are mechanically robust but extracellular matrix materials can also be solubilized and reconstituted into infinite size/shape configurations and tailored to the functional demands of the specific tissue (Cheng et al., 2014; Jones et al., 2016; Moroni et al., 2014).

Effective decellularization of blood vessels can be achieved through physical, chemical, or enzymatic processes; however, each has unique limitations and disadvantages such as the presence of residual chemicals or enzymes and the destruction of essential extracellular matrix (ECM) proteins (Cartmell et al., 2004; Gratzer et al.,

2006; Pu et al., 2018). Chemical decellularization, for example, has been successfully achieved through the use of anionic detergents such as SDS and SDC. These homogeneously disrupting surfactants solubilize cell membranes by inducing curvature stress and thinning the hydrophobic core of the membrane (Nazari et al., 2012). Additional decellularization methodologies have combined different detergents or additional chemical agents with enzymes to effectively target both the cell membrane and nuclear material (Gilpin et al., 2017; Partington et al., 2013). Enzymes including proteases and nucleases are advantageous in decellularization protocols because of their substrate specificities; however, exposure to some enzymes at high concentrations or for prolonged periods can damage collagen or significantly reduce the glycosaminoglycan (GAG) content (Brown et al., 2011; Maghsoudlou et al., 2013; Partington et al., 2013). These materials play a vital role in the mechanical properties of blood vessels, which are deterministic in graft procedure outcomes (Prim et al., 2016).

Many tissue-engineered decellularization strategies that fail to preserve the biochemical and biomechanical properties of native tissues possess poor cell repopulation and differentiation rates (Ahmed et al., 2021). Assuming that the optimal decellularized vascular graft retains properties analogous to its native composition, our broad aim is to use a data-driven approach to develop an optimized decellularization protocol for small-diameter blood vessels to produce vascular scaffolds with properties mirroring that of native tissue. The objectives of this chapter are: (1) to examine the extent of decellularization in the porcine internal thoracic artery (ITA) using an enzymatic-detergent approach, and (2) to present a standard decellularization protocol to effectively develop small-diameter blood vessels for off-the-shelf use in vascular bypass procedures.

Achieving these objectives will contribute to the broader field of tissue engineering through the development of an acellular scaffold which could be used to investigate cellular repopulation and tissue remodeling with applications in vascular bypass grafting procedures.

2.2 Materials and Methods

2.2.1 Tissue Procurement and Enzyme-Detergent Decellularization

Adult porcine ITAs were obtained from a local abattoir and transported to the laboratory in phosphate-buffered saline containing antibiotics (100 units/ml penicillin, 100 mg/ml streptomycin, 1 mg/ml amphotericin-B, and 10 ng/ml gentamicin). The vessels were separated into proximal and distal halves with only the proximal half used in this study due to variations in the structural and mechanical properties along the length of the porcine ITA (Kostelnik et al., 2020). The vessels were cut into 3 cm lengths, placed into 50-ml conical tubes, and rinsed in three changes of PBS for 10 minutes each on a rotator at room temperature (20 rpm) to remove any residual blood. The vessel pieces were then incubated overnight in PBS (control group) or distilled water on a conical tube rotator at 4°C (the control sample was incubated in PBS for the duration of the experimental treatments). Following the overnight incubation, the samples were rinsed in PBS twice for 20-30 minutes each. The samples were incubated again overnight in DNase 1 (Roche Diagnostics cat# 10104159001) at a final concentration 1 mg/ml in DNase digestion buffer (10 mM Tris [pH 7.4], 2.5 mM $MgCl_2$, 0.5 mM $CaCl_2$) on a rotator at 4°C. Samples were subsequently rinsed twice for 20-30 minutes in PBS. Rinsed samples were then placed in a detergent solution composed of equal parts SDS and SDC (Liu et al., 2018). Detergent concentrations included: 0% SDS and SDC (hereafter

referred to as 0% detergent), 0.5% SDS plus 0.5% SDC (hereafter referred to as 1% detergent), 1% SDS plus 1% SDC (hereafter referred to as 2% detergent), 1.5% SDS plus 1.5% SDC (hereafter referred to as 3% detergent), and 3% SDS plus 3% SDC (hereafter referred to as 6% detergent). The samples were incubated in the respective detergent concentrations for 24 or 72 h at room temperature on a rotator (all treatments are listed in Table 2.1). All solutions for decellularization contained antibiotics to mitigate contamination. While the nuclease-detergent step in this study differed from previously published reports, (Böer et al., 2011; Crapo et al., 2011; Pellegata et al., 2013) additional experiments were performed to test DNase application before or after detergents or when omitted from the protocol (n = 8 to 12 per group) (Liu et al., 2018; Pu et al., 2018).

2.2.2 DNA Quantification

Control and decellularized vessels were homogenized in DNAzol Reagent (Thermo Fisher Scientific) and the genomic DNA was precipitated from the lysate with ethanol. Then the DNA was solubilized in 8 mM sodium hydroxide. Quantitative measurements of the total DNA content were then determined by the Quant-IT PicoGreen dsDNA Assay Kit (Invitrogen), following the manufacturer's specifications.

2.2.3 Western Blot Analyses

Biochemical analyses were carried out to assess the relative loss of cytoplasmic (α-smooth muscle actin), cell surface (β1 integrin), and basement membrane (laminin) components during the decellularization protocols. Samples were pulverized in liquid nitrogen and incubated in RIPA solution (150 mM sodium chloride, 1% Triton × 100, 0.5% deoxycholate, 0.1% SDS, 1.5 mM ethylenediaminetetraacetic acid, 50 mM Tris, pH 8.0) containing Pierce Protease Inhibitor Mini-Tablets (Thermo Fisher Scientific).

Samples were incubated at 60°C for 10 minutes and were mixed by inversion three times during incubation. The samples were then centrifuged for 20 minutes at 20,000 *g* (4°C) to resolve insoluble debris. Supernatants were moved to new tubes and the total protein concentration was determined with the Pierce BCA (bicinchoninic acid) protein assay (Thermo Fisher Scientific).

Proteins were separated by SDS-polyacrylamide gel electrophoresis (SDS-PAGE) and transferred to nitrocellulose. The nitrocellulose was rinsed in tris-buffered saline containing 0.05% TWEEN 20 (TBS-T) and blocked in TBS-T containing 5% powdered milk. The nitrocellulose was then rinsed in TBS-T and incubated overnight with validated primary polyclonal antibodies against α-smooth muscle actin (Abcam, #ab5694), laminin (Abcam, #ab11575), and β1 integrin (Sigma-Aldrich. #ab1952). The α-smooth muscle actin and laminin primary antibodies were used at a dilution of 1:500 and β1 integrin at a dilution of 1:1000 in TBS-T containing 1% powdered milk. After three washes in TBS-T, the nitrocellulose was incubated in 1:10,000 HRP-conjugated anti-rabbit IgG (Sigma-Aldrich) secondary antibody for 1-2 hours (h). Following additional rinses in TBS-T, immunoblots were developed with the Pierce SuperSignal Western blot detection reagent (Thermo Fisher Scientific) and exposed to x-ray film. Protein standards were used to provide a reliable molecular weight estimation of the protein signals on the transferred blots. The films were scanned using Adobe Photoshop. To confirm the transfer of proteins following the development of immunoblots, the nitrocellulose was incubated in a 0.1% Fast Green solution (0.1 g Fast Green FCF, 100 ml 1% acetic acid) for 3 minutes and rinsed in water to remove excess stain. Staining of the nitrocellulose with Fast Green enabled the visualization of any bound proteins following electrophoresis.

2.2.4 Scanning Electron Microscopy (SEM)

Samples were obtained by cutting approximately 5 mm cross-sectional segments from each vessel/scaffold. Samples were fixed in McDowell Trump's fixative for 2 h followed by rinsing in PBS (3 × 15 minutes) and ultrapure water (3 × 10 minutes). Samples were dehydrated via a graded ethanol series as follows: 15 minutes in 35%, 50%, and 75% ethanol; 2 × 15 minutes in 95% ethanol; and 3 × 30 minutes in 100% ethanol. Samples were then immersed in fresh hexamethyldisilazane (HMDS) twice for 15 minutes. HMDS was decanted, and the samples were left to dry overnight. The samples were then mounted to allow imaging of the vessel wall in cross-section, gold sputter-coated, and imaged on a JEOL JSM-1610PLUS/LA SEM. At least two representative regions of each sample were imaged. The effects of the experimental treatments on the generation of spaces within the samples were analyzed from SEM images using the NIH ImageJ program.

2.2.5 Histology and Immunohistochemistry

Approximately 2 mm cross sectional slices of the treated vessels were fixed overnight at 4°C in 4% paraformaldehyde prepared in PBS. Fixed vessels were rinsed in PBS, processed for paraffin embedding, and sectioned at approximately 5 µm. Tissue sections were stained with 4',6-diamidino-2-phenylindole (DAPI) to analyze DNA content, picrosirius red (PSR) to assay collagen, and Verhoeff-Van Gieson (VVG) stain to assess elastic fibers. For quantitative analyses, eight random photomicrographs were taken circumferentially around the blood vessel wall. The effects of decellularization treatment parameters were quantified using the NIH ImageJ program.

The fluorescent stain, DAPI, was used to evaluate DNA content of control and decellularized tissue sections. The histological sections were heated in the hybridization oven at 60°C for 10 minutes, deparaffinized in xylene, and rehydrated through a descending alcohol series (100%, 95%, 70%). The tissue sections were rinsed twice for 10 minutes each in PBS then incubated in DAPI (1:1000 dilution) in the dark for 30 minutes at room temperature. The sections were subsequently rinsed twice in PBS for 20 minutes each. For quantitative analysis, eight random photomicrographs were taken circumferentially around the vessel wall on a Nikon E600 fluorescence microscope at an exposure time of 2.5 ms. The effects of the decellularization treatment parameters on DAPI-positive content were quantified using ImageJ. Within ImageJ, the photomicrographs were converted to 16-bit grayscale, a constant threshold was set, and the threshold area was measured. This area-based analysis (percent of field) was used to extract and quantify the DAPI-positive nuclear content from the regions of interest.

PSR stain was used to evaluate vascular collagen content of control and decellularized tissue sections. Histological sections were heated to 60°C in a hybridization oven for 45 minutes and deparaffinized using xylenes, a descending alcohol series (100%, 95%, and 70%), and a brief 1-minute bath in distilled water. The sections were stained with 0.2% Phosphomolybdic Acid and then rinsed in distilled water. The sections were then stained with PSR (12 g Picric Acid, 400 ml water, 0.4 g Sirius Red) followed by incubation in 0.1 M HCL. Ascending alcohol (70%, 90%, and 100%) and xylene series were used to dehydrate the sections. The sections were mounted with Depex. The stained sections were imaged, and the collagen volume was determined as described above.

Verhoeff-Van Gieson stain was used to evaluate elastic fiber content of control and decellularized tissue sections. Histological sections were heated at 60°C in hybridization oven for 30 minutes and then deparaffinized using xylenes and a descending alcohol series (100%, 95%, and 70%). The sections were rinsed in distilled water twice, followed by incubation with Working Elastin Stain (10 ml Hematoxylin Solution, 1.5 ml Ferric Chloride Solution, 4 ml Weigert's Iodine Solution, 2.5 ml deionized water) for 10 minutes. Following incubation, the sections were rinsed in distilled water and differentiated in Working Ferric Chloride Solution (3 ml Ferric Chloride Solution and 37 ml distilled water) for 1-2 minutes. The sections were sequentially rinsed briefly in tap water, 95% alcohol to remove the iodine, and Van Gieson for 1-3 minutes. They were again rinsed in 95% alcohol, dehydrated in xylene, and cover slipped. The stained sections were imaged, and the vascular elastic fiber density was determined as described above.

2.2.6 Biochemical Quantification of Glycosaminoglycan (GAG) Content

A dimethylmethylene blue (DMMB) assay was used to evaluate the sulfated-GAG (sGAG) content within treated ITA samples. The tissue samples were dried in glass tubes at 65°C overnight in a hybridization oven and the dried tissues were weighed. Tissues were digested with Papain (Invitrogen cat# 10108014001) made in Papain Extraction Buffer (400 mg Sodium Acetate, 200 mg EDTA, 40 mg Cysteine HCl – added to 50 ml 0.2 M NaH_2PO_4) overnight at 65°C. The liquid was transferred to Eppendorf tubes and centrifuged for 10 minutes at 10,000 g (4°C). Aliquots of each sample were added to the DMMB Reagent (16 mg DMMB, 3.04 g Glycine, 1.6 g Sodium Chloride, 95 ml 0.1 M Acetic acid – for 1 L). sGAG concentrations relative to dry tissue weight were

determined by comparison to a standard curve using a BioRad Benchmark Plus Microplate Spectrophotometer at 525 nm.

2.2.7 Mechanical Testing

The mechanical properties of the fresh, control, and decellularized ITAs were determined through biaxial inflation-extension testing using a Bose Bio-Dynamic mechanical testing device following protocols described previously (Kostelnik et al., 2020). The tissue sections were trimmed to comply with the testing device's 10 mm maximum displacement range, mounted onto two luer-fittings, and then fixed in place with 3–0 braided sutures. Then tissues were submerged in a testing bath and perfused with 1% PBS and sodium nitroprusside (10^{-5} M) to elicit a fully passivated state (Zhou et al., 2018). The "in vivo axial stretch ratio" was found by axial stretching the vessel to a point that yielded a constant axial force value in response to pressurization. Every decellularized tissue sample then underwent f5 cycles of extension and inflation preconditioning to minimize viscous dissipation and ensuring reproducible results. For data collection, all vessels were inflated from 0 to 200 mmHg while measurements of force, axial stretch, and outer diameter were collected every 20 mmHg at the in vivo axial stretch ratio as well as 10% above and below that value.

2.2.8 Statistical Analysis

Comparisons of the histological images, SEM images, and the mechanical properties between the anionic detergent concentrations and the controls were made via one-way ANOVA followed by Tukey's Multiple Comparison post hoc test. Data were imported into Prism GraphPad for statistical analyses. Statistically significant differences were taken at a level of $p < 0.05$.

2.3 Results and Discussion

The objective of decellularization is to maximize cell and cellular debris removal while minimizing alterations to the native properties of the ECM during treatment. A successfully optimized chemical decellularization protocol for small-diameter vascular repair would be a large step forward in the tissue engineering field.

Currently, there is no widely agreed upon method for evaluating the extent of decellularization. This is largely due to the fact that the cell density, ECM composition, and stiffness, amongst other characteristics, is different from one tissue to another, and therefore, decellularization methods and techniques must be specifically tailored to the tissue of interest (Mendibil et al., 2020). However, Crapo's group suggested that the following characteristics define a fully decellularized material:

1. Less than 50 ng of double-stranded DNA per mg ECM dry weight
2. No visible nuclear material in tissue sections after DAPI and/or H&E staining
3. DNA fragment length of less than 200 base pairs

In this study, we focused on the first two criteria by performing DNA quantitation and DAPI staining on porcine internal thoracic arteries following detergent treatment.

Six different treatments of porcine internal thoracic arteries were used to investigate the differential response of varying SDS and SDC anionic detergent concentrations (0% – 6% total detergent concentration) after 24 and 72 h in the presence of DNase.

2.3.1 Decellularization Efficiency – DNA Quantification

The effects of anionic detergent (SDS and SDC) concentration and treatment duration on decellularization efficiency were evaluated by staining of tissue sections with

DAPI to assess DNA content. Representative sections from the tunica media can be seen in Figure 2.1. Treatment of the porcine ITAs with DNase 1 followed by anionic detergents for 24 h resulted in substantial DAPI-positive material in the scaffolds that were not statistically different from the untreated controls (Figure 2.1A). Interestingly, unlike the control samples, the DAPI-positive material was no longer in compact nuclei but more diffusely organized. Anionic detergent treatment for 72 h resulted in undetectable DAPI staining (Figure 2.1B). There were no significant differences between the concentrations of anionic detergent at 72 h. The PicoGreen assay also failed to reveal significant differences in DNA concentration for any groups after only 24 h (Figure 2.2A). However, the 72 h treatment resulted in a significant decrease in the measured DNA concentration between all treated and untreated controls (Figure 2.2B) with no significant differences between the detergent concentrations. To further evaluate decellularization efficiency and to examine differential effects on specific tissue components (i.e., cytoplasmic, cell surface, and ECM), western blot analyses were carried out of tissue lysates following treatment (Figure 2.3). For these experiments, western blots were performed of representative cytoplasmic (α-smooth muscle actin), cell surface (β1 integrin), and basement membrane (laminin) proteins. Quantitative assessment was not performed due to a lack of normalization control. Despite this limitation, it was clear that the inclusion of high concentrations of an anionic detergent (2%–6%) effectively removed cytoplasmic and cell surface proteins after 24 and 72 h of treatment. After 24 h of detergent treatment, a high concentration of laminin was still detected in the tissue lysates, but this diminished substantially following 72 h of treatment.

Others have shown that low concentrations of anionic detergents can effectively remove cellular material from vascular tissue with minimal detergent retention (Gratzer et al., 2006; Pu et al., 2018). Analysis of the cellular content in our vessels revealed that the porcine ITAs retained DAPI-positive material even after 24 h of treatment with high levels of anionic detergent treatment. This was undetectable when the treatment duration was extended to 72 h, as seen in Figure 2.1B. The quantified residual DNA concentrations using PicoGreen for both treatment durations match the DAPI image thresholding, which supports our findings that nuclease and low anionic detergent concentration treatment for 72 h was preferred over 24 h for removing significant nuclear content. However, it should be acknowledged that a limitation of the study was that we did not optimize the concentrations of the SDS and SDC detergents independently. It should also be noted that the nuclease-detergent sequence within our protocol was different from other studies (Böer et al., 2011; Pellegata et al., 2013).; however, DNase is frequently fully omitted from decellularization protocols (Lieu et al., 2018; Pu et al., 2018). Yet, additional experiments were performed in our lab to test DNase application before or after detergents or when omitted from the protocol. Our findings revealed similar residual DNA concentrations irrespective of enzyme-detergent order but were significantly less than when DNase was omitted from the protocol altogether (Figure 2.4). Furthermore, qualitative analysis of cytoplasmic and surface proteins confirmed that 24 h of detergent treatment removed a large amount of cellular material while 72 h showed a significant cellularity decrease of all groups in a concentration-independent manner. However, extending the treatment duration to 72 h reduced laminin, a basement membrane protein, in the scaffolds. This reduction in

laminin could have adverse effects on the recellularization of scaffolds as vascular cells readily adhere to this protein and coating decellularized platforms with laminin enhances recellularization (Toshmatova et al., 2019). Another acknowledged limitation of our study is that increasing detergent concentration and time could increase the risk of detergent retention within the scaffolds. This would present a concern with cytotoxicity and would limit the efficacy of any future recellularization; however, we did not test this directly.

2.3.2 Effects of Detergent Concentration and Time – Scaffold Structure

Scanning electron microscopy was performed to analyze the effects of anionic detergent concentration and treatment duration on the structure of the treated scaffolds (Figure 2.5). Treatment of the porcine ITAs resulted in the formation of pores between ECM fibers within the tissue tunica media. At 24 and 72 h, the area fraction of porosity within the tissue was significantly greater in the samples treated with detergent compared to the non-detergent treated samples (Figure 2.5C, D). For the 24 h detergent treatment, the highest doses of detergent (3% and 6%) detergent created a significantly greater porosity when compared to the lower doses (1% and 2%); however, this difference was no longer evident after 72 h of treatment and all detergent conditions were statistically the same.

Analysis of the scaffold structure following anionic detergent treatment revealed an inversely proportional increase in tissue porosity with detergent and DNase treatments which is consistent with other research groups (Brown et al., 2011). While our study did not test this, we hypothesized that the recellularization process would be enhanced by the increased porosity of the tissues during culture as cells and nutrients may more readily

diffuse throughout the matrix; however, this increase in porosity also presents a concern with tissue swelling and could be a potential site for residual detergents to reside (Gratzer et al., 2006; Pu et al., 2018). Similarly, the DNase-enzyme detergent protocol used in our study could also influence the retention of residual detergents.

2.3.3 Effects of Detergent Concentration and Time – ECM Content

Various assays qualitatively measured the collagen, elastin, and sGAG content to assess the effects of anionic detergent concentration and treatment duration on the vascular ECM. Overall collagen content was inferred by analyzing the hydroxyproline content for all experimental groups, while collagen distribution and area fraction were histologically evaluated using PSR. There was substantial heterogeneity in the effects of detergent treatment on collagen content with both assays (Figure 2.6). There was no significant effect of detergent concentration and treatment duration on the overall collagen content (Figure 2.6), partly due to the level of variability.

Through quantitative analysis of the VVG stain, it is evident that there was no significant effect of detergent concentration nor treatment duration on elastic fiber content (Figure 2.7). Interestingly, there was a trend toward increased elastic fiber density following treatment for 24 or 72 h with higher concentrations of detergents. This suggests compaction of the elastic fibers due to removal of the cells and other components with the conditions involving the higher concentrations of detergents.

The most notable alteration to the vascular ECM was the significant reduction in sGAG concentration with all decellularization treatments compared to the control samples (Figure 2.8). A reduction in sGAG concentration was also seen in samples treated only with DNase 1 (0% detergent).

Analysis of the constituent makeup of the decellularized ITAs did not reveal significant differences in the two major load-bearing proteins, namely collagen and elastin, following anionic detergent and DNase treatments. Retention of these ECM proteins throughout the decellularization process are crucial for maintaining the tissue integrity and providing attachment sites for recellularization. Although we did not test differentially for collagen type IV compared to other types, the persistence of overall collagen and the retention of laminin, as previously discussed, at short treatment durations suggests a high potential for recellularization.

While it was apparent that there were no significant differences in the ECM proteins, collagen and elastin, there was a significant decrease in sGAG content. sGAGs are complex anionic unbranched heteropolysaccharides that represent major structural and functional ECM components of connective tissues. sGAGs participate in a number of vascular events including regulation of vascular permeability, lipid metabolism, and thrombosis, but also play a critical role in cell growth, differentiation, and function (Uhl et al., 2020; Lepedda et al., 2021). While our study only quantified sGAG concentration, a deeper knowledge of the structural complexity of sGAGs is necessary as this is what accounts for their numerous functions; however, this still presents challenges, but is also an opportunity to take major steps forward in the field of vascular tissue engineering.

2.3.4 Effects of Detergent Concentration and Time – Biomechanical Properties

Inflation and extension biaxial tests were performed to quantify the physical characteristics of the scaffolds and used to determine how anionic detergent concentrations impacted the vascular wall mechanical properties. All tissues were tested at common axial stretches to facilitate comparisons between groups. Overall, the control

and fresh vessels exhibited similar mechanical properties and the presence of detergents impacted the slope of the stress-strain curve (stiffness), but in a concentration-independent manner. This means that the presence of anionic detergents had some effect, but no obvious trends emerged between the varying concentrations on mechanical properties. When the anionic detergent treatment duration was increased to 72 h the tissue appeared to exhibit a more compliant stress-strain profile.

Although our group performed a complete mechanical characterization via state-of-the-art biaxial testing protocols using matched tissue segments, very few of the metrics used for mechanical comparison reached statistical significance (Figures 2.9, 2.10). Others have shown that decellularized arteries are significantly stiffer than native tissue through uniaxial tensile testing, but these studies fail to assess how decellularization impacts the multidirectional loading of these arteries (Williams et al., 2009). A decrease in the cellularity of these engineered tissue constructs is accompanied by a decrease in cell-ECM fiber interactions. It is important to point out that longer decellularization treatment durations resulted in more compliant stress-strain profiles relative to the control group. We believe the compliant response seen with prolonged detergent-based decellularization procedures (>24 h) may be due in part to greater disruption of the ECM fiber network, decreased fiber-fiber interactions, or collagen denaturation and structural changes (Gratzer et al., 2006; Williams et al., 2009; Hwang et al., 2017).

2.4 Conclusions

In our study, short-term (24 h) detergent treatments in conjunction with DNase failed to remove sufficient nuclear material; however, prolonged treatment (72 h) resulted in adequate decellularization even when using low concentrations of anionic detergents

(1% detergent). Based on these results, the combination of enzymatic and anionic detergent decellularization of porcine ITAs revealed the removal of cellular content proceeded in a time-dependent and concentration-independent manner. Significant differences in tissue composition and structure were found through a combination of qualitative and quantitative analyses of histology, electron microscopy, and biaxial mechanical testing. Collectively, these findings suggest that low detergent concentrations for 72 h can be used in future decellularization strategies, but at the cost of some altered mechanical properties and laminin retention. Moving forward, these differences can be used to optimize the decellularization process of xenogeneic vascular tissue and may contribute to the development of an acellular scaffold used to investigate cellular repopulation and tissue remodeling.

Table 2.1: List of Detergent Decellularization Treatments

Treatment	Treatment Description	Duration
Control	PBS	24 and 72 h
0% detergent	0% SDS and SDC	24 and 72 h
1% detergent	0.5% SDS plus 0.5% SDC	24 and 72 h
2% detergent	1% SDS plus 1% SDC	24 and 72 h
3% detergent	1.5% SDS plus 1.5% SDC	24 and 72 h
6% detergent	3% SDS plus 3% SDC	24 and 72 h

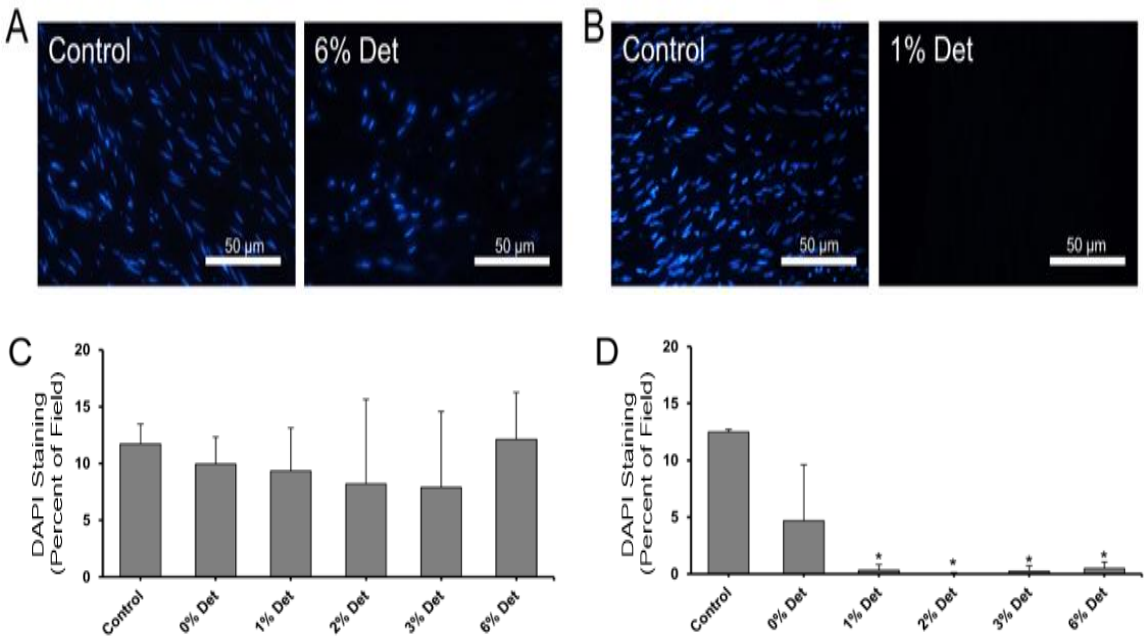

Figure 2.1 – DAPI stain following (A) 24 h and (B) 72 h of anionic detergent treatment. The insets are representative images of DAPI-stained sections of control, 6% detergent-treated, and 1% detergent-treated tissues at respective time points. Area fraction quantification of DAPI-positive pixels for (C) 24 h and (D) 72 h. Statistical significance between detergent concentrations relative to untreated controls was determined by one-way ANOVA and is indicated (*) at $p < 0.05$. Mean ± SD, $n = 4$ for each group.

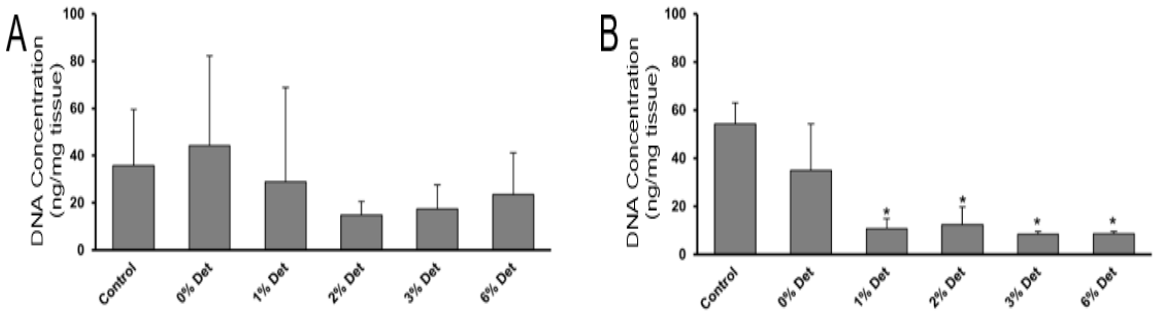

Figure 2.2 – Quantification of DNA content from PicoGreen assays following (A) 24 h and (B) 72 h of anionic detergent treatment. Statistical significance between detergent concentrations relative to untreated controls was determined by one-way ANOVA and is indicated by (*) at $p < 0.05$. Mean ± SD, $n = 4$ for each group.

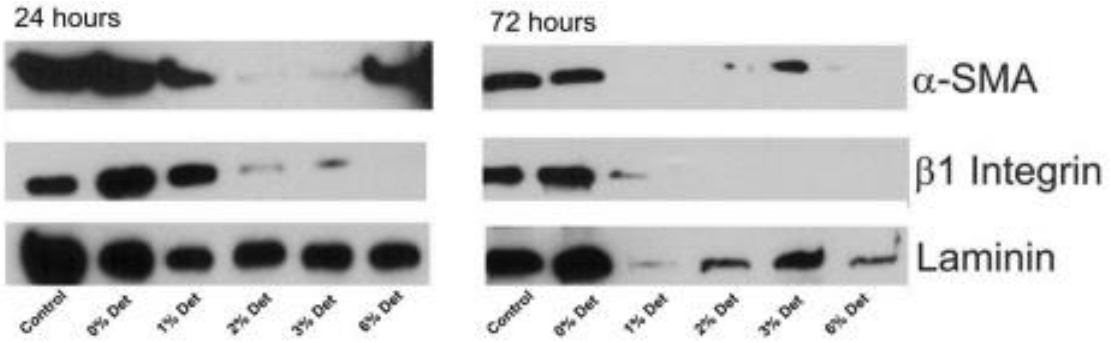

Figure 2.3 – Western blot analysis of representative cytoplasmic (α-smooth muscle actin, cell surface (β1 integrin), and basement membrane (laminin) proteins. Representative images of western blots illustrating the effects of anionic detergent concentration and treatment duration. Lanes 1–6 are untreated control, 0% detergent, 1% detergent, 2% detergent, 3% detergent, and 6% detergent, respectively.

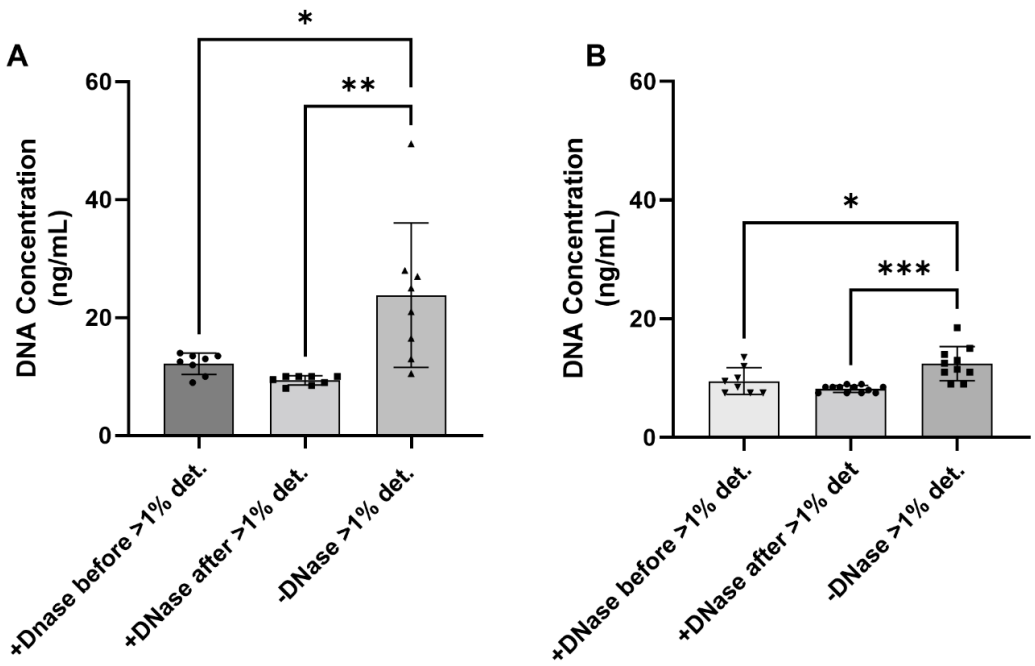

Figure 2.4 – Quantified PicoGreen DNA concentrations for (A) 24 h and (B) 72 h samples treated with DNase (+DNase) before or after detergents or when DNase was omitted from the protocol (-DNase). Statistical significance was given by (*,**,***) at $p < 0.05$, $p < 0.01$, and $p < 0.001$ respectively. Mean ± STD (n = 8 to 12 per group).

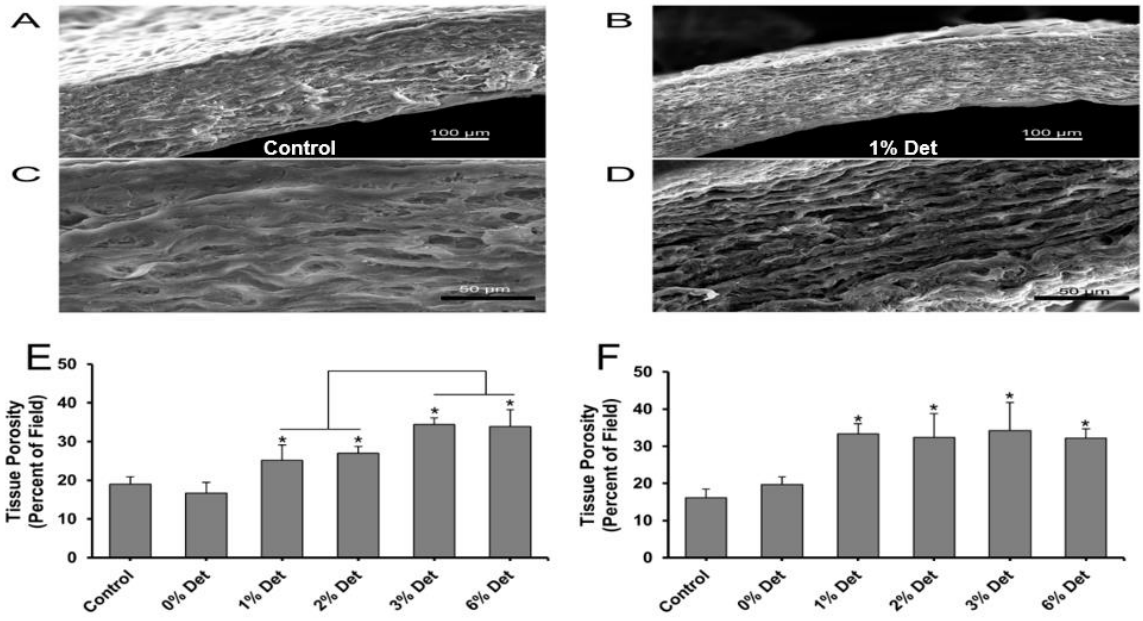

Figure 2.5 – Representative scanning electron microscopic images of (A,C) 72 h control sample at low and high power (B, D) 1% detergent for 72 h at low and high power. Quantification of the total porosity in tissues after (E) 24 h and (F) 72 h for all anionic detergents was performed on high-powered images. Statistical significance between detergent concentrations relative to untreated controls was determined by one-way ANOVA and is indicated by (*) at $p < 0.05$. Mean ± SD, $n = 3$ for each group.

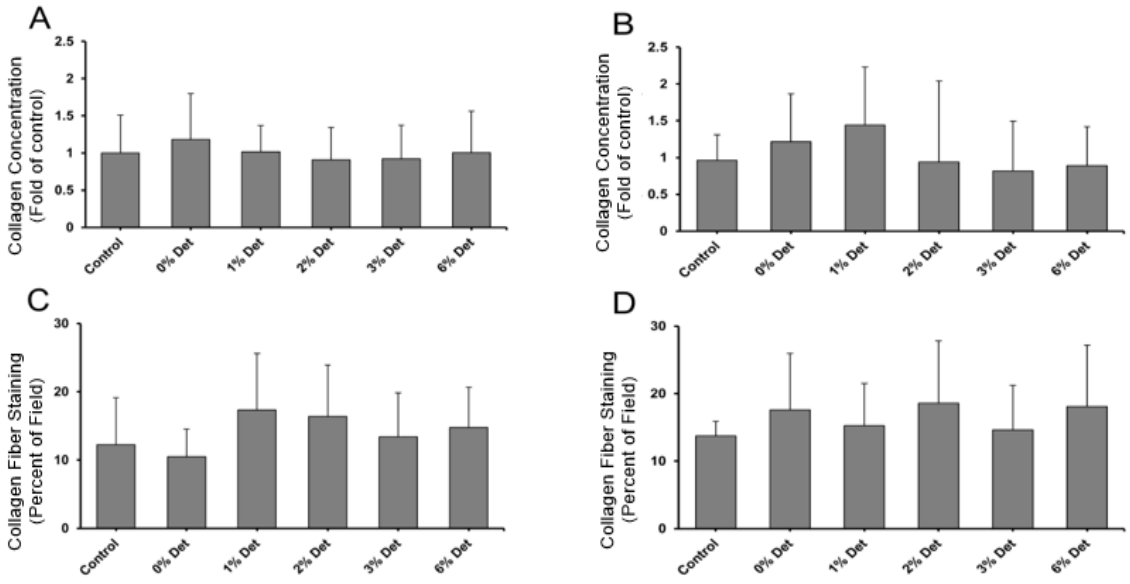

Figure 2.6 – Quantification of hydroxyproline concentrations after (A) 24 h and (B) 72 h of anionic detergent treatment. Collagen percent volume quantified by image thresholding of PSR-stained tissue sections after treatment of (C) 24 h and (D) 72 h. No statistically significant differences were found following ANOVA analysis. Mean ± SD, $n = 5$ for each group.

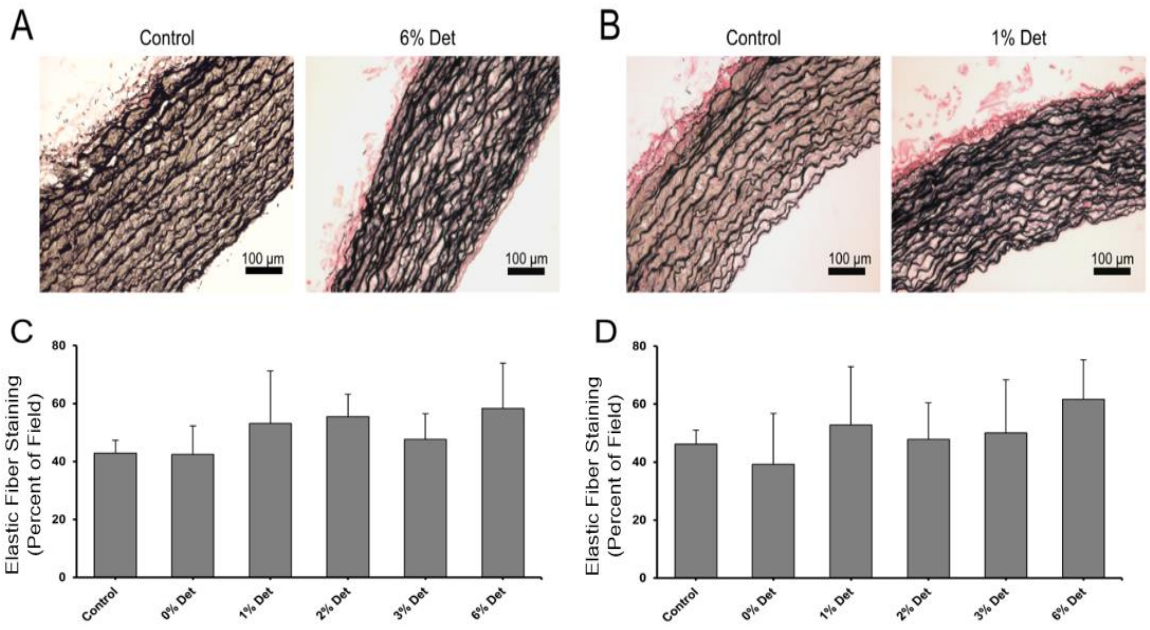

Figure 2.7 – Quantitative analysis of elastic fibers following anionic detergent treatment. Representative microscopic images of control samples, 6% detergent, and 1% detergent for (A) 24 h and (B) 72 h, respectively. Elastic fiber area fraction was quantified from VVG-stained tissue following anionic detergent treatment for (C) and (D) 72 h. No statistically significant differences were found following ANOVA analysis. Mean ± SD, n = 5 for each group.

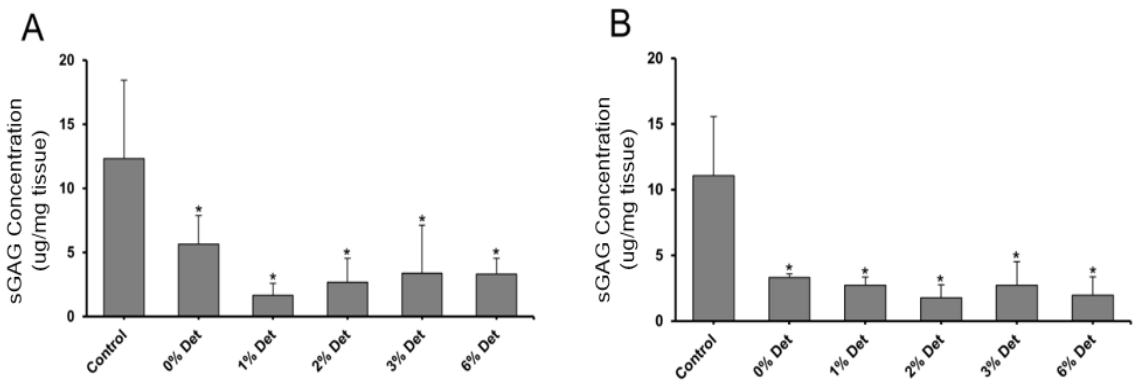

Figure 2.8 – Analysis of dimethylmethylene blue (DMMB) concentrations of all anionic detergent concentrations following (A) 24 h and (B) 72 h of treatment. DMMB concentration was indicative of the glycosaminoglycan concentration present in all tissue samples. Statistical significance between detergent concentrations relative to untreated controls was determined by one-way ANOVA and is indicated by (*) at $p < 0.05$. Mean ± SD, $n = 5$ for each group.

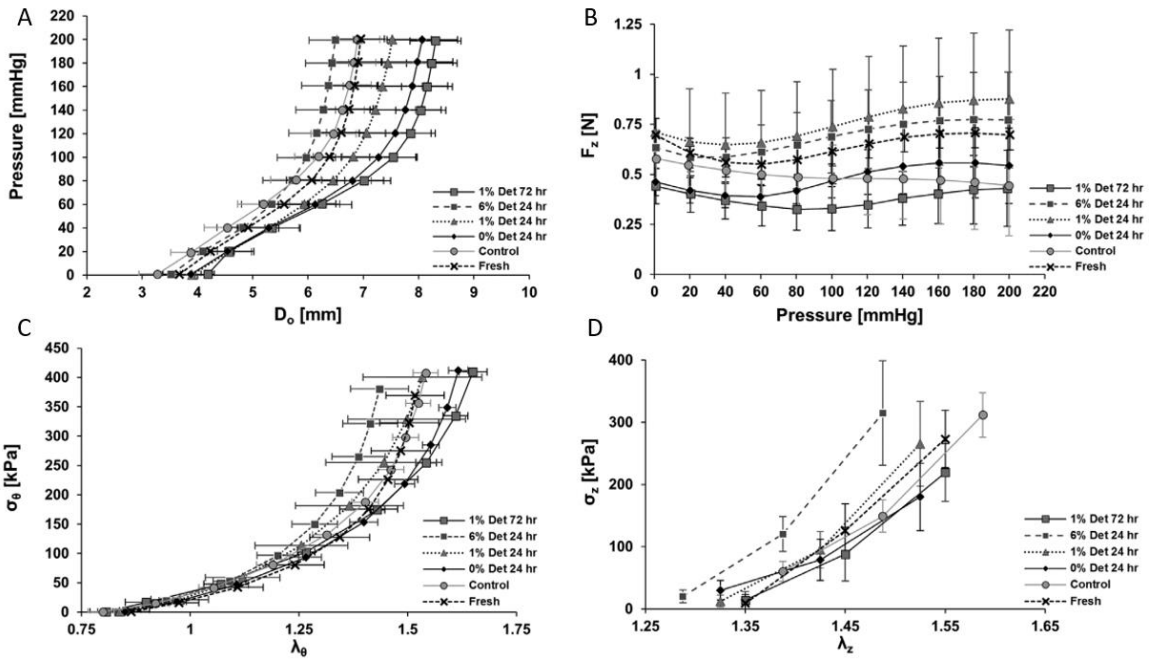

Figure 2.9 – Biaxial mechanical data for all decellularization groups and fresh porcine ITA tissue. (A) Pressure-outer diameter, (B) axial force-pressure, (C) circumferential stress-stretch all plotted at $\lambda_z = 1.45$, (D) axial stress-stretch at 100 mmHg. Mean ± SD, *n* = 4 for each group.

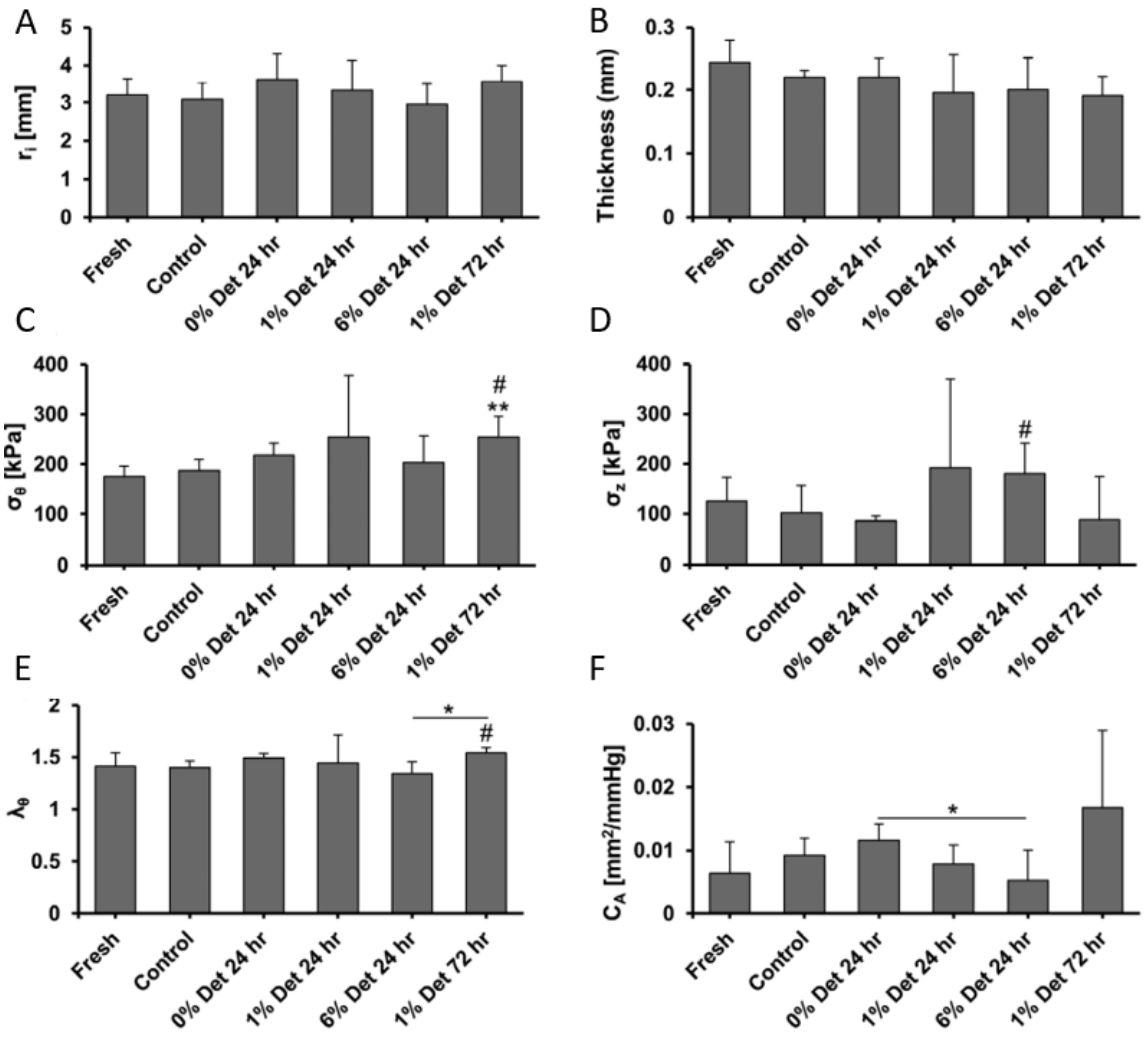

Figure 2.10 – Biaxial mechanical data of decellularized porcine ITAs plotted at common loading conditions of 100 mmHg and $\lambda_z = 1.45$. (A) Inner radius, (B) thickness, (C) circumferential stress, (D) axial stress, (E) circumferential stretch, and (F) area compliance. Statistical significance between different decellularized treatments is indicated by (*) at $p < 0.05$. Statistical significance between a decellularized ITA group and the control or fresh tissue is indicated by (#) and (**), respectively. Mean ± SD, $n = 4$ for each group.

CHAPTER 3

DECELLULARIZATION OF PORCINE INTERNAL THORACIC ARTERIES USING SUPERCRITICAL CARBON DIOXIDE

3.1 Introduction

As previously discussed in Chapter 2, approximately 400,000 bypass surgeries are carried out annually in the United States alone (Go et al., 2014; Li et al., 2014), leading to a pressing need for more effective, readily available vascular replacement materials. This is particularly the case for small-diameter vessels (<6 mm internal diameter) such as the coronary arteries, as synthetic grafts possess low long-term patency due to increased thrombogenicity and insufficient compliance homogeneity between the native vessel and synthetic grafts. As mentioned previously, a common approach for vascular replacement surgery is the use of autografts, or the patient's own vessels; however, such vessels are limited by availability if previously used and are subject to pathological remodeling called vein graft disease. Currently, tissue-engineered vascular graft replacements are urgently needed and have been the subject of widespread investigation.

Decellularized extracellular matrices (dECM) from xenogeneic vascular tissues have received considerable attention as scaffolds for tissue engineering. dECM offer many unique advantages such as preservation of tissue-specific extracellular matrix (ECM) microstructure and composition, demonstration of tissue-mimetic mechanical properties, and retention of biochemical cues in favor of subsequent recellularization

(Pawan et al., 2019). However, current processes of decellularization still face several challenges including the need for balance between cell removal and ECM preservation, the deleterious and cytotoxic effects of chemical detergents used for decellularization on the native ECM architecture, and the prolonged periods of time required for decellularization processing. The need to overcome these obstacles has led to an extensive search for novel decellularization practices.

To address the deficiencies of more traditional chemical and physical decellularization methods, treatment with supercritical carbon dioxide ($scCO_2$) has gained popularity as a novel and more innovative approach (Guler et al., 2017; Casali et al., 2018; Harris et al., 2021). $scCO_2$ is relatively non-toxic, non-flammable, and is chemically inert. It has a relatively low critical temperature (31°C) making it viable at physiologic temperatures, and possesses desirable transport properties including low viscosity, high density and diffusivity, and leaves no residual solvents. One area of tissue engineering (TE) in which $scCO_2$ has been used extensively is in the fabrication of TE scaffolds from synthetic polymers by polymer foaming (Tai et al., 2007; Floren et al., 2011). $scCO_2$ has also been used in other biomedical applications including sterilization of synthetic and natural biomaterials (White et al., 2006; Donati et al., 2012; Santos-Rosales et al., 2022), pasteurization (Fleury et al., 2018; Bertolini et al., 2020), and extraction of biological molecules and compounds (Crampon et al., 2011; Molino et al., 2019).

It has recently been demonstrated that utilization of $scCO_2$ holds great potential for decellularization of tissue scaffolds. Specifically, a novel method incorporating $scCO_2$ has been shown to fully decellularize porcine aorta and preserve aortic mechanical

properties (Casali et al., 2018). In addition to the reduction in harmful chemical detergents, $scCO_2$ offers a significantly shorter decellularization process, on the order of hours instead of days to weeks, as evidenced by the Casali *et al.* study. However, the parameters of the Casali *et al.* $scCO_2$ method (e.g., SDS concentration and treatment time, $scCO_2$ treatment time, and depressurization rate) were not optimized.

Our broad aim is to develop a novel optimized $scCO_2$ decellularization protocol that will give rise to a more time-efficient decellularization method and will yield a small-diameter vascular scaffold with enhanced structural, biomechanical, and biochemical properties compared to those of the enzyme-detergent methods described in Chapter 2. The objectives of this chapter are: (1) to examine the extent of decellularization in the porcine internal thoracic artery (ITA) using a hybrid chemical detergent-$scCO_2$ approach; (2) to optimize detergent concentrations in which the scaffolds will be exposed to the least amount of detergent possible to sufficiently decellularize and to maintain native tissue properties prior to $scCO_2$ treatment; and (3) to present a standard hybrid detergent-$scCO_2$ protocol that decellularizes porcine ITAs more quickly and as efficiently as the previously described enzyme-detergent methods to ultimately develop small-diameter blood vessels for off-the-shelf use in vascular bypass procedures. Achieving these objectives will have huge implications for tissue engineering and clinical application in vascular bypass grafting, as it will provide the foundation for high throughput production of vascular replacement materials and addresses a critical clinical need.

3.2 Materials and Methods

3.2.1 Tissue Procurement and Hybrid Detergent/Supercritical CO_2 Decellularization

Adult porcine ITAs were obtained from a local abattoir and transported to the laboratory in phosphate-buffered saline containing antibiotics (100 units/ml penicillin, 100 mg/ml streptomycin, 1 mg/ml amphotericin-B, and 10 ng/ml gentamicin). The vessels were separated into proximal and distal halves with only the distal half used in this study. The vessels were cut into 3 cm lengths, placed into 50-ml conical tubes, and rinsed in three changes of PBS for 10 minutes each on a rotator at room temperature (20 rpm) to remove any residual blood. One vessel piece (native sample) was then removed and stored for end assays. The remaining vessel pieces were then incubated overnight in PBS on a conical tube rotator at 4°C. Following overnight incubation, two vessel pieces (PBS only and PBS + supercritical CO_2) were removed and incubated in PBS for the duration of the experimental treatments. The remaining samples were incubated again overnight in DNase 1 (Roche Diagnostics cat# 10104159001) at a final concentration 500 ug/ml in DNase digestion buffer (10 mM Tris [pH 7.4], 2.5 mM $MgCl_2$, 0.5 mM $CaCl_2$) on a rotator at 4°C. Samples were subsequently rinsed in three changes of PBS for 30 minutes each. Again, two vessel pieces (DNase and DNase + supercritical CO_2) were removed and stored in a new conical tube of PBS at 4°C. The two remaining rinsed samples were then placed in a detergent solution composed of 0.5% SDS and incubated for 2 or 24 h at room temperature on a rotator (all treatments are listed in Table 3.1). All solutions for decellularization contained antibiotics to mitigate contamination. Respective samples were then treated with scCO_2 for 1 h as described in Table 3.1

The respective porcine ITA segment was loaded into the treatment chamber (8) of the $scCO_2$ apparatus, shown in Figure 3.1. The apparatus contained valves and fittings rated for high pressures up to 68.9 MPa (2). Liquid carbon dioxide (1) was compressed in a chilled syringe pump (3) and slowly bubbled into the presaturation chamber (6) to maximize mass transfer. In this chamber, water and $scCO_2$ were stirred vigorously until reaching thermodynamic equilibrium as to presaturate the $scCO_2$ and maintain the matrix hydration state of the tissue upon contact. Once equilibrium was reached, the valve to the treatment chamber was opened, and $scCO_2$ was allowed to contact the tissue. During treatment, the environmental chamber (5) was used to maintain the temperature at 40°C, and the back-pressure regulator was used to keep the pressure of the $scCO_2$ in the vessels constant at 13.8 MPa (2000 psi). After the tissue was treated with $scCO_2$ for 1 h, a manual hand pump (12) was used to slowly depressurize the system. Each sample treated with $scCO_2$ was loaded into the apparatus and treated individually. These methods were adapted from the Casali group and applied to our porcine ITAs (Casali et al., 2018).

3.2.2 DNA Quantification

Small samples of blood vessel (approx. 4 mg) were homogenized in DNAzol Reagent (Thermo Fisher Scientific) and the genomic DNA was precipitated from the lysate with ethanol. Then the DNA was solubilized in 8 mM sodium hydroxide. Quantitative measurements of the total DNA content were then determined by the Quant-IT PicoGreen dsDNA Assay Kit (Invitrogen), following the manufacturer's specifications.

3.2.3 Western Blot Analyses

Biochemical analyses were carried out to assess the relative loss of cytoplasmic (α-smooth muscle actin), cell surface (β1 integrin), and basement membrane (laminin) components during the decellularization protocols. Samples (approx. 4 mg) were pulverized in liquid nitrogen and incubated in RIPA solution (150 mM sodium chloride, 1% Triton × 100, 0.5% deoxycholate, 0.1% SDS, 1.5 mM ethylenediaminetetraacetic acid, 50 mM Tris, pH 8.0) containing Pierce Protease Inhibitor Mini-Tablets (Thermo Fisher Scientific). Samples were incubated at 60°C for 10 minutes and were mixed by inversion three times during incubation. The samples were then centrifuged for 20 minutes at 20,000 *g* (4°C) to resolve insoluble debris. Supernatants were moved to new tubes and the total protein concentration was determined with the Pierce BCA (bicinchoninic acid) protein assay (Thermo Fisher Scientific).

Proteins were separated by SDS-polyacrylamide gel electrophoresis (SDS-PAGE) and transferred to nitrocellulose. The nitrocellulose was rinsed in tris-buffered saline containing 0.05% TWEEN 20 (TBS-T) and blocked in TBS-T containing 5% powdered milk. The nitrocellulose was then rinsed in TBS-T and incubated overnight with validated primary polyclonal antibodies against α-smooth muscle actin (Abcam, #ab5694), laminin (Abcam, #ab11575), and β1 integrin (Sigma-Aldrich. #ab1952). The α-smooth muscle actin and laminin primary antibodies were used at a dilution of 1:500 and β1 integrin at a dilution of 1:1000 in TBS-T containing 1% powdered milk. After three washes in TBS-T, the nitrocellulose was incubated in 1:10,000 HRP-conjugated anti-rabbit IgG (Sigma-Aldrich) secondary antibody for 1-2 hours (h). Following additional rinses in TBS-T, immunoblots were developed with the Pierce SuperSignal Western blot detection reagent

(Thermo Fisher Scientific) and exposed to x-ray film. Protein standards were used to provide a reliable molecular weight estimation of the protein signals on the transferred blots. The films were scanned using Adobe Photoshop. To confirm the transfer of proteins following the development of immunoblots, the nitrocellulose was incubated in a 0.1% Fast Green solution (0.1 g Fast Green FCF, 100 ml 1% acetic acid) for 3 minutes and rinsed in water to remove excess stain. Staining of the nitrocellulose with Fast Green enabled the visualization of any bound proteins following electrophoresis.

3.2.4 Scanning Electron Microscopy (SEM)

Samples were obtained by cutting approximately 5 mm cross-sectional segments from each vessel/scaffold. Samples were fixed in 2.5% glutaraldehyde for 2 h followed by rinsing in PBS (3 × 15 minutes) and ultrapure water (3 × 10 minutes). Samples were fixed in 1% osmium tetroxide (OsO_4) for one hour followed by PBS rinse. Following rinsing, samples were immersed in 1% tannic acid for one hour. The PBS rinse and 1% OsO_4-fixation steps were then repeated. Tissue was again rinsed in PBS followed by one hour 1% tannic acid rinse. Samples were then rinsed in PBS and fixed with 1% OsO_4 for a third time followed by a water rinse. Samples were then dehydrated via a graded ethanol series as follows: 2 × 15 minutes in 70% ethanol; 2 × 15 minutes in 95% ethanol; and 2 × 30 minutes in 100% ethanol. Samples were next dehydrated by critical point drying using a Samdri-PVT-3B critical point dryer. The samples were mounted to allow imaging of the vessel wall in cross-section, gold sputter-coated, and imaged on a JEOL JSM-IT100 SEM. At least two representative regions of each sample were imaged.

3.2.5 Histology and Immunohistochemistry

Approximately 2 mm cross sectional slices of the treated vessels were fixed overnight at 4°C in 4% paraformaldehyde prepared in PBS. Fixed vessels were rinsed in PBS, processed for paraffin embedding, and sectioned at approximately 5 µm. Tissue sections were stained with 4',6-diamidino-2-phenylindole (DAPI) to analyze DNA content, picrosirius red (PSR) to assay collagen, and Verhoeff-Van Gieson (VVG) stain to assess elastic fibers. For quantitative analyses, eight random photomicrographs were taken circumferentially around the blood vessel wall. The effects of decellularization treatment parameters were quantified using the NIH ImageJ program. The fluorescent stain, DAPI, was used to evaluate DNA content of control and decellularized tissue sections. The histological sections were heated in the hybridization oven at 60°C for 10 minutes, deparaffinized in xylene, and rehydrated through a descending alcohol series (100%, 95%, 70%). The tissue sections were rinsed twice for 10 minutes each in PBS then incubated in DAPI (1:1000 dilution) in the dark for 30 minutes at room temperature. The sections were subsequently rinsed twice in PBS for 20 minutes each. For quantitative analysis, eight random photomicrographs were taken circumferentially around the vessel wall on a Nikon E600 fluorescence microscope at an exposure time of 2.5 ms. The effects of the decellularization treatment parameters on DAPI-positive content were quantified using ImageJ. Within ImageJ, the photomicrographs were converted to 16-bit grayscale, a constant threshold was set, and the threshold area was measured. This area-based analysis (percent of field) was used to extract and quantify the DAPI-positive nuclear content from the regions of interest.

PSR stain was used to evaluate vascular collagen content of control and decellularized tissue sections. Histological sections were heated to 60°C in a hybridization oven for 45 minutes and deparaffinized using xylenes, a descending alcohol series (100%, 95%, and 70%), and a brief 1-minute bath in distilled water. The sections were stained with 0.2% Phosphomolybdic Acid and then rinsed in distilled water. The sections were then stained with PSR (12 g Picric Acid, 400 ml water, 0.4 g Sirius Red) followed by incubation in 0.1 M HCL. Ascending alcohol (70%, 90%, and 100%) and xylene series were used to dehydrate the sections. The sections were mounted with Depex. The stained sections were imaged, and the collagen volume was determined as described above.

Verhoeff-Van Gieson stain was used to evaluate elastic fiber content of control and decellularized tissue sections. Histological sections were heated at 60°C in hybridization oven for 30 minutes and then deparaffinized using xylenes and a descending alcohol series (100%, 95%, and 70%). The sections were rinsed in distilled water twice, followed by incubation with Working Elastin Stain (10 ml Hematoxylin Solution, 1.5 ml Ferric Chloride Solution, 4 ml Weigert's Iodine Solution, 2.5 ml deionized water) for 10 minutes. Following incubation, the sections were rinsed in distilled water and differentiated in Working Ferric Chloride Solution (3 ml Ferric Chloride Solution and 37 ml distilled water) for 1-2 minutes. The sections were sequentially rinsed briefly in tap water, 95% alcohol to remove the iodine, and Van Gieson for 1-3 minutes. They were again rinsed in 95% alcohol, dehydrated in xylene, and cover slipped. The stained sections were imaged, and the vascular elastic fiber density was determined as described above.

3.2.6 Biochemical Quantification of Glycosaminoglycan (GAG) Content

A dimethylmethylene blue (DMMB) assay was used to evaluate the sulfated-GAG (sGAG) content within treated ITA samples. The tissue samples were dried in glass tubes at 65°C overnight in a hybridization oven and the dried tissues were weighed. Tissues were digested with Papain (Invitrogen cat# 10108014001) made in Papain Extraction Buffer (400 mg Sodium Acetate, 200 mg EDTA, 40 mg Cysteine HCl – added to 50 ml 0.2 M NaH_2PO_4) overnight at 65°C. The liquid was transferred to Eppendorf tubes and centrifuged for 10 minutes at 10,000 g (4°C). Aliquots of each sample were added to the DMMB Reagent (16 mg DMMB, 3.04 g Glycine, 1.6 g Sodium Chloride, 95 ml 0.1 M Acetic acid – for 1 L). sGAG concentrations relative to dry tissue weight were determined by comparison to a standard curve using a BioRad Benchmark Plus Microplate Spectrophotometer at 525 nm.

3.2.7 Residual SDS Quantification

An SDS Detection and Estimation Kit (Thermo Fischer Scientific) was used to quantify residual SDS from the native, control, and hybrid-treated tissue. The samples were first homogenized in water. The assay then involved mixing 500 µl of methylene blue dye with 250 µl extraction buffer and 5 µl of the homogenized sample, then vortexing for 30 seconds. 1 mL of chloroform was then added, and the mixture was vortexed again for 30 seconds. If SDS is present, methylene blue is extracted into the organic phase. After a 5 minute incubation, the bottom chloroform phase was sampled and residual SDS was quantified by comparison to a standard curve using a BioRad Benchmark Plus Microplate Spectrophotometer at 600 nm.

3.2.8 Mechanical Testing

The mechanical properties of the fresh, control, and decellularized ITAs were determined through biaxial inflation-extension testing using a Bose Bio-Dynamic mechanical testing device following protocols described previously (Kostelnik et al., 2021). The tissue sections were trimmed to comply with the testing device's 10 mm maximum displacement range, mounted onto two luer-fittings, and then fixed in place with 3–0 braided sutures. Then tissues were submerged in a testing bath and perfused with 1% PBS and sodium nitroprusside (10^{-5} M) to elicit a fully passivated state (Zhou et al., 2018). The "in vivo axial stretch ratio" was found by axial stretching the vessel to a point that yielded a constant axial force value in response to pressurization. Every decellularized tissue sample then underwent f5 cycles of extension and inflation preconditioning to minimize viscous dissipation and ensuring reproducible results. For data collection, all vessels were inflated from 0 to 200 mmHg while measurements of force, axial stretch, and outer diameter were collected every 20 mmHg at the in vivo axial stretch ratio as well as 10% above and below that value.

3.2.9 Statistical Analysis

Comparisons of the histological images, SEM images, and the mechanical properties between the anionic detergent concentrations and the controls were made via one-way ANOVA followed by Tukey's Multiple Comparison post hoc test. Data were imported into Prism GraphPad for statistical analyses. Statistically significant differences were taken at a level of $p < 0.05$.

3.3 Results and Discussion

Many chemical and physical decellularization processes have been proposed to efficiently isolate the ECM of a tissue from its inhabiting cells while maintaining the biochemical and biomechanical properties of the native tissue. However, these methods are time-consuming, utilize harsh chemicals that can denature ECM proteins, and often fail to remove residual detergent that can provoke cell cytotoxicity. Hence, supercritical CO_2 has received attention as a novel alternative strategy for tissue decellularization to potentially alleviate these problems; however, this strategy has been evaluated in limited tissue types and methods are far from optimized with this approach.

In this study, we focused on developing a novel optimized $scCO_2$ decellularization protocol that would lead to a more time-efficient decellularization method and would yield a small-diameter vascular scaffold with enhanced structural, biomechanical, and biochemical properties compared to the decellularized scaffold products generated with chemical methods alone. As indicated in Table 3.1, the experimental conditions utilized in the present study were established to evaluate the effects of $scCO_2$, DNase, and SDS alone or in combination on porcine ITA decellularization. These treatments were compared to an untreated control (samples incubated in PBS without anionic detergent nor $scCO_2$ treatment) and to native porcine ITA samples. Our previous study (Chapter 2) indicated that full decellularization of porcine ITAs was accomplished after treatment in DNase overnight followed by 72 hours of treatment with 1% anionic detergent. Preliminary studies suggest that residual SDS remains in these samples even after extensive rinses in PBS (data not shown). Based upon these results and published literature, we hypothesized that inclusion of $scCO_2$ in the treatment protocol will enhance

decellularization of the tissue and allow utilization of lower detergent concentrations or durations of treatment. Based on this, we selected to evaluate inclusion of 0.5% SDS for 2 and 24 hours.

3.3.1 Decellularization Efficiency – DNA Quantification

While there is no current universal standard determining "full decellularization" of tissue, we utilized the parameters suggested by Crapo *et al.* and evaluated DNA content both by DAPI staining and biochemical analysis (Crapo et al., 2011). Representative sections from the tunica media stained with DAPI can be seen in Figures 3.2 and 3.3. There was a significant decrease in DAPI-positive material between untreated controls and porcine ITAs treated with DNase 1 alone, DNase plus $scCO_2$, DNase plus 24 hours of 0.5% SDS, and DNase plus 24 hours of 0.5% SDS plus $scCO_2$ (Figure 3.2). $scCO_2$ alone had no effect on DAPI-positive staining. Quantitative comparison of DAPI staining illustrated a slight, but insignificant decrease in all samples treated with $scCO_2$ relative to their counterparts (the same condition without $scCO_2$).

The effects of reducing the duration of treatment with SDS from 24 h to 2 h on DNA content were then evaluated. As expected, anionic detergent treatment for 2 h alone resulted in an increase in DAPI-positive material when compared to ITAs treated for 24 h. There was a significant decrease in DAPI-positive material present between the 2 h detergent treatment plus $scCO_2$ and the native tissue; however, no condition was significantly different from the untreated controls (Figure 3.3). Treatment with anionic detergent for 2 h plus $scCO_2$ resulted in a significant decrease in DAPI-positive material when compared to 2 h anionic detergent treatment alone, also shown in Figure 3.3

While there was a decrease in the measured DNA concentration, the PicoGreen assay did not reveal significant differences in the measured DNA concentration between either 24 and 2 h detergent treatment plus $scCO_2$ and untreated controls (Figure 3.4). There was, however, a significant decrease in the DNA concentration between samples treated with 24 h detergent alone and 24 h detergent plus $scCO_2$ and native tissue. There was also a significant decrease in DNA concentration between native tissue and porcine ITAs treated with DNase 1 alone, DNase plus $scCO_2$, DNase plus 2 h of 0.5% SDS and DNase plus 2 h of 0.5% SDS plus $scCO_2$. Like the DAPI staining, $scCO_2$ alone had no effect on DNA concentration measured by PicoGreen.

To further evaluate decellularization efficiency and to examine differential effects on specific tissue components (i.e., cytoplasmic, cell surface, and ECM), western blot analyses were carried out of tissue lysates following treatment (Figure 3.5). For these experiments, western blots were performed of representative cytoplasmic (α-smooth muscle actin), cell surface (β1 integrin), and basement membrane (laminin) proteins. Quantitative assessment was not performed due to a lack of normalization control. Despite this limitation, it was clear that treatment of samples with $scCO_2$ alone resulted in decreased levels of all three proteins relative to control samples. Similarly, treatment with DNase 1 plus $scCO_2$ decreased the levels of all three proteins relative to DNase 1 alone. Inclusion of 0.5% SDS for 2 h in the treatment protocol, with or without $scCO_2$, resulted in α-SMA and β1 integrin being undetectable. Interestingly, while treatment with 0.5% SDS resulted in decreased laminin levels, inclusion of $scCO_2$ resulted in an apparent increase in retention of this protein in samples.

The conclusions drawn from the analysis of the cellular content in our vessels treated with the hybrid method at varying detergent concentrations are twofold. First, Figure 3.4 shows a level of DNA removal similar to our previous detergent-enzyme decellularization study (Chapter 2), below the suggested threshold for adequate decellularization, with either 2 or 24 h of detergent plus an hour of $scCO_2$ treatment. While shown earlier by Casali *et al*. in porcine aorta (Casali et al., 2018), we have now demonstrated that a hybrid method, which we adapted and applied to the porcine ITA, is able to achieve our initial objective: to present a hybrid detergent-$scCO_2$ protocol that decellularizes porcine ITAs more quickly and as efficiently as our previously described enzyme-detergent methods. Second, our results have shown that treatment with a low concentration of detergent (0.5% SDS) for as little as 2 h plus $scCO_2$ can effectively decellularize porcine ITAs. Not only does this accelerate the decellularization process, but it also reduces the time in SDS and is an even lower concentration of detergent than the lowest concentration presented in our detergent-enzyme decellularization study (Chapter 2). These findings can be explained by the known mechanisms of how detergents and supercritical fluids interact with cells and ECM proteins. It is well established that most ionic detergents, including SDS, solubilize both external and nuclear membranes (Seddon et al., 2004). This leads to intracellular contents exiting the cell and leaving behind cellular debris. However, detergent alone will not remove cellular debris from the matrix, which explains the need for either prolonged rinsing following detergent only treatments or subsequent exposure to $scCO_2$ after treatment with reduced concentrations of detergent. Nevertheless, this could explain why it took 72 h plus days of extensive rinsing to decellularize with 1% detergent in Chapter 2. This is also critically

important because, while SDS can efficiently remove nuclear and cytoplasmic content, it tends to denature proteins and can alter the native structure of the matrix at high concentrations or when exposed to tissues for extended periods of time. It can also be difficult to rid tissues of cytotoxic residual SDS following extended periods in detergent solutions.

It is noteworthy that the concentration of measured DNA in the untreated control tissues in both the 2 and 24 h groups was already below the suggested decellularization criterion of 50 ng dsDNA per mg ECM dry weight prior to any treatment. This is an unusual finding, as the literature demonstrates measured DNA well above that criterion using the PicoGreen assay in a variety of control tissues in other studies (e.g., porcine aorta, murine pancreas, human saphenous vein) prior to decellularization treatments (Goh et al., 2013; Casali et al., 2018; Suleiman et al., 2021). It is possible that the amount of porcine ITA tissue (3-5 mg) used in our study to measure DNA content using the PicoGreen assay was not enough to efficiently recover DNA from the samples.

This protocol could not be fully optimized due to this limitation; however, these results are encouraging that 2 h detergent treatment plus $scCO_2$ could be used in future porcine ITA decellularization studies. Additional studies should be conducted to assess the DNA content of porcine ITAs in larger tissue samples. Nonetheless, the maintenance of native ECM properties and reducing residual SDS within the scaffolds treated with 2 h detergent plus $scCO_2$ were exciting results and will both be discussed in a subsequent section of this chapter. Similar to results seen in Chapter 2, treatment with 0.5% SDS alone for both 2 and 24 h resulted in DAPI-positive material that was no longer in compact nuclei form but was more diffusely organized. This could account for the

inconsistencies seen between results of the DAPI staining and the DNA concentration measured by the PicoGreen assay particularly following the 2 h detergent treatment. Following this assessment of the decellularization efficiency, the remaining parts of the study were conducted using the 2 h 0.5% SDS treatment plus scCO2 hybrid protocol.

Furthermore, qualitative analysis of cytoplasmic and cell surface proteins confirmed that inclusion of $scCO_2$, particularly when combined with treatment with a low concentration of detergent for 2 h, removed a large amount of cellular material. Likewise, treatment with 2 h of detergent treatment plus 1 h of $scCO_2$ reduced the basement membrane protein laminin in the scaffolds. Moreover, it appeared that treatment with $scCO_2$ independent of its combination with detergent also reduced laminin compared to the untreated controls, and this was a consistent finding amongst the western blots that were run for laminin protein (n = 5). Conversely, detergent treatment plus $scCO_2$ increased when compared to detergent alone yet this was not a consistent finding. As mentioned in the last chapter, reduction or removal could have adverse effects on the recellularization of scaffolds as vascular cells readily adhere to this protein and coating decellularized platforms with laminin enhances recellularization (Toshmatova et al., 2019).

3.3.2 Effects of SDS/$scCO_2$ Hybrid Treatment – Scaffold Structure

Scanning electron microscopy was performed on a small number of samples to visualize any gross effects of the SDS/$scCO_2$ hybrid treatment on the structure of the treated scaffolds (Figure 3.6). From these samples, the vascular wall appears to be compact with little spaces in the control samples (Figure 3.6A). This is similar to SEM analysis of control samples in Chapter 2. In contrast, treatment with 0.5% SDS, with or

without $scCO_2$, resulted in the generation of spaces or pores within the blood vessel wall, likely due to removal of cells. Again, this is similar to our previous SEM of vessels decellularized with detergent alone (Chapter 2). Due to time constraints, a small number of samples were analyzed in the present study and morphometric analyses were not performed to quantitatively assess structural changes including tissue porosity or ECM organization. Although we did not perform these tests and were unable to confirm this ourselves, SEM from one study showed that the fibrous network of $scCO_2$-decellularized collagen scaffolds, including porcine artery, heart, and kidney, are not altered demonstrating the mild nature of the $scCO_2$ decellularization process (Hsieh et al., 2020).

3.3.3 Effects of SDS/$scCO_2$ Hybrid Treatment – ECM Content

Assays were carried out to qualitatively measure collagen, elastin, and sGAG content to assess the effects of the SDS/$scCO_2$ hybrid treatment on the vascular ECM. Overall collagen content was inferred by analyzing the hydroxyproline content for all experimental groups, while collagen distribution and area fraction were histologically evaluated with picrosirius red (PSR). There was a trend toward increased collagen fiber density with all of the experimental treatments relative to the PBS-treated controls. This was the greatest in the 2 h detergent alone and 2 h of detergent plus $scCO_2$ treatment (Figure 3.7). However, none of these changes were statistically significant. As we have previously seen with elastic fiber density, the increased density of collagen fibers seen by microscopic analysis is likely due to compaction of the decellularized tissues following removal of cells and cellular proteins. This increase in collagen density has been observed in decellularization studies of various tissue types including porcine aorta and liver (Baptista et al., 2011; Hazwani et al., 2019). A similar trend toward increased

collagen concentration following treatment was also seen with the hydroxyproline assay; however, there was a reduction in collagen concentration, albeit insignificant, in the condition pretreated with detergent and exposed to 1 h of $scCO_2$ (Figure 3.7).

Elastic fiber density was histologically evaluated by staining tissue sections with Verhoeff-Van Gieson (VVG) stain. Through quantitative analysis of the VVG stain, it was evident that there was no significant effect of the SDS/$scCO_2$ hybrid treatment on elastic fiber content (Figure 3.8). Interestingly, there remained a slight trend toward increased elastic fiber density in each of the decellularized samples compared to the untreated control. This again suggests compaction of the elastic fibers due to removal of cells and other components with the conditions involving pretreatment outside of $scCO_2$ alone.

The DMMB assay was utilized to measure sGAG concentration in porcine ITA samples. While there was no statistically significant difference across any of the conditions analyzed, there appeared to be an increase in sGAG concentration in the samples treated with detergent alone and with detergent plus $scCO_2$. There was substantial heterogeneity in sGAG concentration in all of the remaining samples and the significance of this increase in the detergent-treated samples is presently unclear (Figure 3.9). Nonetheless, it directly contradicts the results from our detergent-enzyme decellularization study (Chapter 2) where sGAG concentration was diminished in the decellularization process.

Analysis of the constituent makeup of the decellularized ITAs did not reveal significant differences in the two major load-bearing proteins, collagen and elastin, following DNase and anionic detergent treatments with or without $scCO_2$. While the

hydroxyproline assay used to biochemically assess collagen concentration within the scaffolds revealed a decrease in collagen content within the samples treated with detergent plus $scCO_2$ when compared to the untreated control and to the sample treated with detergent alone, this difference was not seen when histologically evaluated using PSR, a stain used to evaluate collagen distribution and area fraction. On the contrary, PSR staining revealed an increase in collagen fiber density in all conditions when compared to the untreated control. Because PSR identifies fibrillar collagen networks and is used to distinguish between collagen types I and III, it is plausible that other types of collagen, such as collagen type IV, are lost following treatment with detergent plus $scCO_2$ and this could be the difference that is reflected in the results of the hydroxyproline assay. However, it is also possible that the $scCO_2$ treatment plays a role in collagen loss as this trend is not apparent in the tissue treated with detergent alone. Global comparison of the ECM composition of decellularized scaffolds and native tissue by proteomic analysis would be advantageous to assess which specific ECM proteins are more susceptible to loss compared to others.

While it was apparent that there were no significant differences in the ECM proteins, collagen and elastin, there was a substantial, but insignificant, increase in sGAG concentration between scaffolds treated with detergent and detergent plus $scCO_2$ and the untreated control. This is an unusual finding, as exposure to anionic detergents is powerful in removing sGAGs, therefore destroying ECM rigidity and function (White et al., 2017; Neishabouri et al., 2022). Several studies, including a previous one of our own, have reported deleterious effects of SDS upon GAG content (Brown et al., 2011; Ren et al., 2013; Faulk et al., 2014; Kostelnik et al., 2021). Because of this, it has become

common for protocols to use detergents at low concentrations over extended periods of time to minimize ECM damage while eventually removing all cellular material (Sierad et al., 2015). Interestingly, a reduction in sGAG concentration was also seen in samples treated only with DNase 1 (0% detergent) in our previous study suggesting that the DNase 1 plus detergent treatment in the current study might also reduce sGAG, yet this was not the case. We hypothesized that using low concentrations of detergent for a short duration coupled with $scCO_2$ treatment could possibly maintain, but not increase sGAG concentration when compared to untreated controls. Histological assessment of sGAG distribution using Alcian Blue staining would be useful to confirm the biochemical results of our DMMB assay. The DMMB assay simply quantifies sGAGs; however, extensive study is still required to assess more accurately which GAG subtypes are lost during decellularization and the role they each play in cell signaling, which serves to modulate a vast number of biochemical processes (Raman et al., 2005).

3.3.4 Effects of SDS/$scCO_2$ Hybrid Treatment – Residual SDS

Removal of SDS is another criterion for successful decellularized ECM (dECM) utilization and scaffold viability, as different cells have varying thresholds for SDS-based detergent-induced cytotoxicity (Zvarova et al., 2016). According to Zvarova *et al*., the cytotoxic threshold observed for many cell types is a concentration greater than 0.002% SDS (Zvarova et al., 2016). Residual SDS was quantified for the SDS/$scCO_2$ hybrid treatment, and the results can be seen in Figure 3.10. These results show that 2 h of detergent (0.5% SDS) treatment plus 1 hour of $scCO_2$ reduces SDS concentration below the cytotoxic level of 0.002% when compared to samples treated with 0.5% SDS alone. This result suggests that our SDS/$scCO_2$-treated scaffolds could potentially promote an

environment conducive to cell growth and proliferation upon repopulation. This is an exciting finding as $scCO_2$ could compare even more favorably than PBS washes for extended periods of time.

3.3.5 Effects of SDS/$scCO_2$ Hybrid Treatment – Biomechanical Properties

Inflation and extension biaxial tests were performed to analyze the physical characteristics of treated porcine ITA scaffolds and used to determine how the SDS/$scCO_2$ hybrid treatment impacted the vascular wall mechanical properties. Due to unforeseen loss of vessels during testing, this set only included the following conditions: Native, PBS + 1 h $scCO_2$, DNase + 1 h $scCO_2$, 0.5% SDS, 0.5% SDS + 1 h $scCO_2$. These specimens were tested at common axial stretches to facilitate comparison between the groups. Continuous data is plotted in Figure 3.11 to show how the outer diameter and axial force change throughout the entire pressure range of 0-200 mmHg. Figure 3.11C depicts the impact of the SDS/$scCO_2$ hybrid treatments on the slope of the stress-strain curve (stiffness). At common loading conditions, there appeared to be an increase in circumferential stress in the DNase + 1 h $scCO_2$, 0.5% SDS, and 0.5% SDS + 1 h $scCO_2$ conditions when compared to the native tissue. Conversely, there was a noticeable decrease in axial stress in all conditions treated with $scCO_2$. Likewise, a decrease in area compliance was also observed in all $scCO_2$-treated conditions. These results can be seen in Figure 3.12. It is difficult to draw any conclusions with an incomplete set of treated tissue and sample size of $n = 1$ for the existing groups. Despite this obvious limitation, these discrete biaxial data taken from a common load (100 mmHg) will allow us to quantify if there are any significant differences existing between groups when we have a large enough sample size. It may also be interesting to include destructive testing to

evaluate burst pressure and suture retention, which are used to determine a scaffold's ability for reimplantation. However, it is important to note that several studies looking for an alternative to chemical and enzymatic processes have recently shown that mammalian tissues can be successfully decellularized with $scCO_2$, providing ECM scaffolds with improved mechanical properties that could be used to promote cell growth and angiogenesis (Sawada et al., 2008; Balestrini et al., 2016; Huang et al., 2017; Casali et al., 2018; Seo et al., 2018; Harris et al., 2021). Overall, a more thorough characterization of the biomechanical properties following treatment with the SDS/$scCO_2$ hybrid method is necessary to confirm whether or not our hybrid protocol maintains the mechanical properties of the native tissue.

3.4 Conclusions

While not fully optimized, a more efficient method for decellularizing porcine ITAs utilizing $scCO_2$ has been presented for use in the decellularization of porcine ITAs. Our SDS/$scCO_2$ hybrid protocol has not only reduced the time tissue is exposed to detergent but has also significantly decreased the concentration of detergent required to pretreat the tissues. This method appears to offer considerably faster decellularization of tissues (2 hours of 0.5% SDS plus one hour of $scCO_2$) without requiring long-term exposure to detergents as presented in Chapter 2. In our study, both the 2 h and 24 h SDS/$scCO_2$ hybrid treatments removed sufficient nuclear material. Because these conditions yielded similar results, we continued our experiments using the 2 h SDS/$scCO_2$ hybrid treatment as to prevent the tissue from exposure to detergent for longer than is necessary to achieve adequate decellularization. Based on these results, the combination of anionic detergent plus $scCO_2$ decellularization of porcine ITAs revealed

the removal of cellular content proceeded in a manner dependent upon both pretreatment with detergent followed by treatment with $scCO_2$. While few significant differences were seen, trends in tissue composition and structure could be observed through a combination of qualitative and quantitative analysis of histology and biochemical analyses. Collectively, these findings suggest that very low detergent concentrations coupled with $scCO_2$ treatment can be used in future decellularization strategies, but at the cost of some laminin retention. However, further study is required to determine the possibilities and limitations of this method, including bioactivity studies, testing $scCO_2$-generated scaffolds as replacement material in animal models, and assessing biochemical modification of the scaffolds.

Table 3.1: List of Hybrid Detergent-scCO$_2$ Treatments

	Treatment Description			
Treatment Name	**PBS**	**DNase 1**	**0.5% SDS**	**scCO$_2$**
Native	30 m, stored at 4°C			
PBS (only)	Duration of experiment at 4°C			
PBS + 1 h scCO2	24 h at 4°C			1 h
DNase	24 h at 4°C	24 h		
DNase + 1 h scCO2	24 h at 4°C	24 h		1 h
0.5% SDS	24 h at 4°C	24 h	24 h	
0.5% SDS + 1 h scCO$_2$	24 h at 4°C	24 h	24 h	1 h

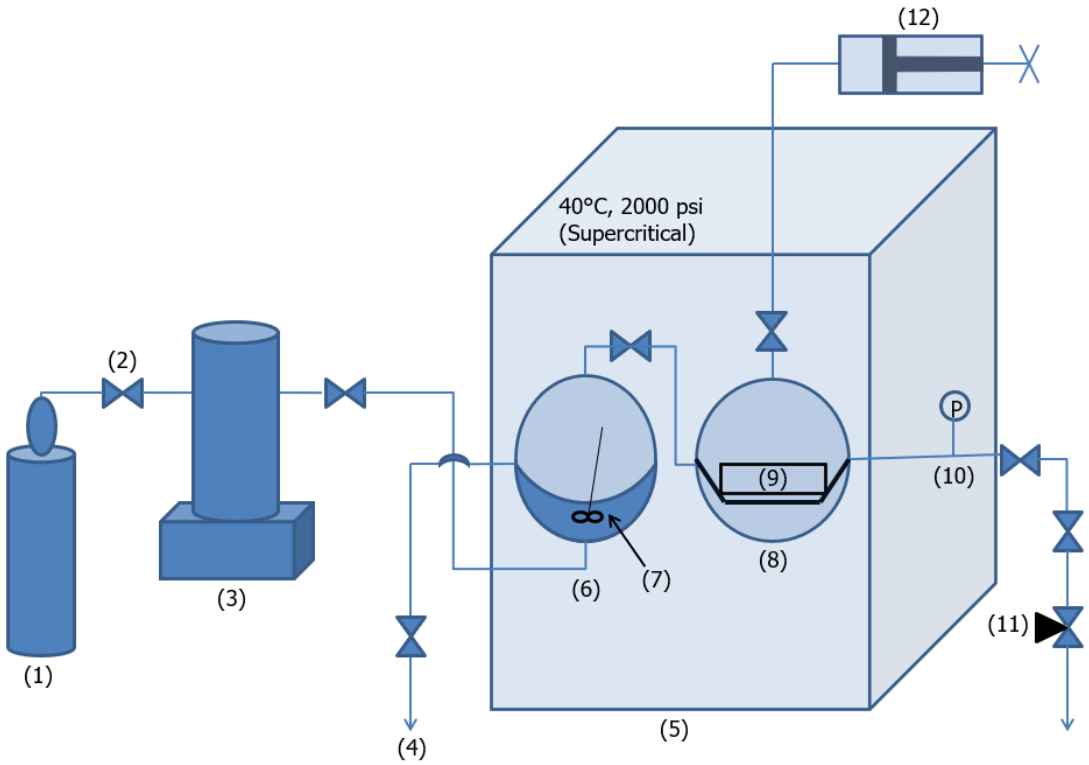

Figure 3.1 – Supercritical CO_2 Decellularization Schematic: (1) – CO_2 cylinder; (2) – High Pressure Valve; (3) – Syringe Pump; (4) – Backup Vent; (5) – Environmental Chamber; (6) – Presaturation Chamber; (7) – Stirring bar and water; (8) – Treatment Chamber; (9) – Porcine ITA sample; (10) – Pressure Gauge; (11) – Back-Pressure Regulator; (12) – Manual Hand Pump (Schematic adapted from Casali et al., 2018).

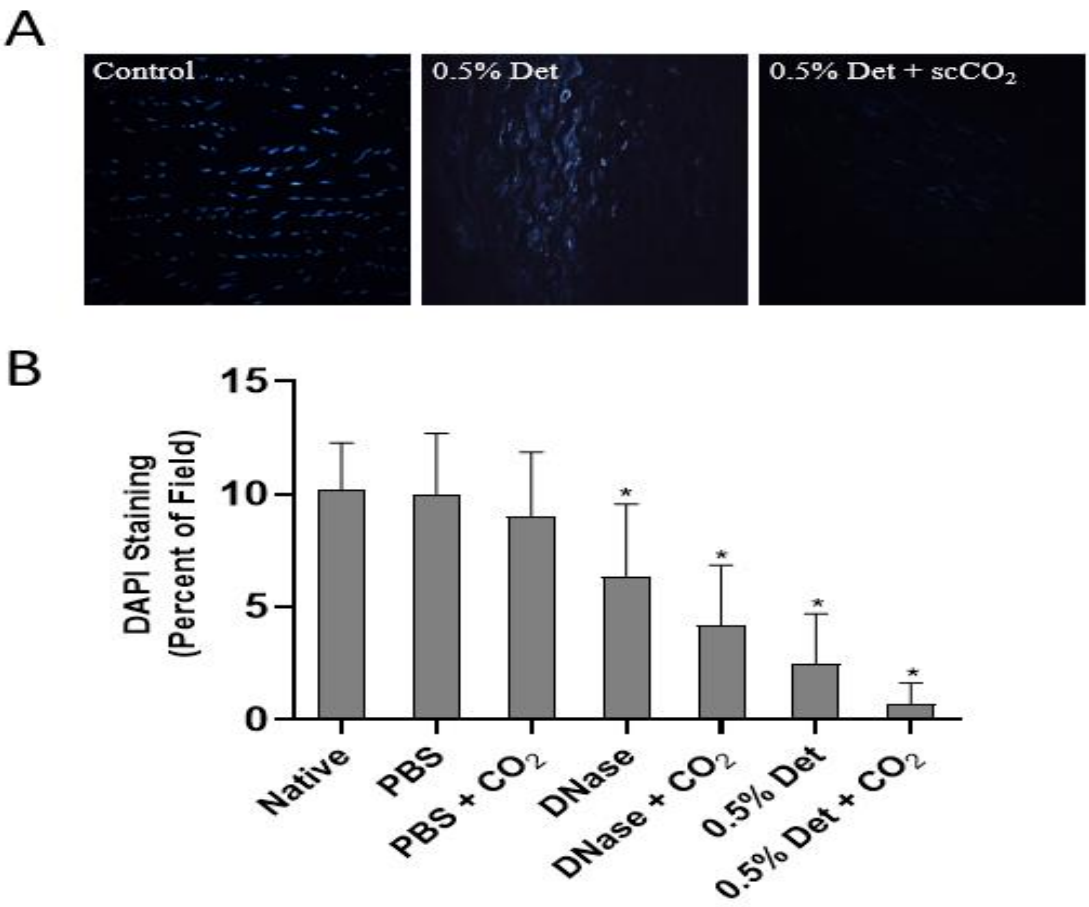

Figure 3.2 – DAPI stain following 24 h of anionic detergent treatment followed by one hour of $scCO_2$ treatment (A). The insets are representative images of DAPI-stained sections of PBS (control), 0.5% detergent-treated, and 0.5% detergent + $scCO_2$-treated tissues. Area fraction quantification of DAPI-positive pixels (B). Statistical significance between treatments and relative to untreated controls was determined by one-way ANOVA and is indicated by (*) at $p < 0.05$. Mean ± SD, $n = 18$ for each group.

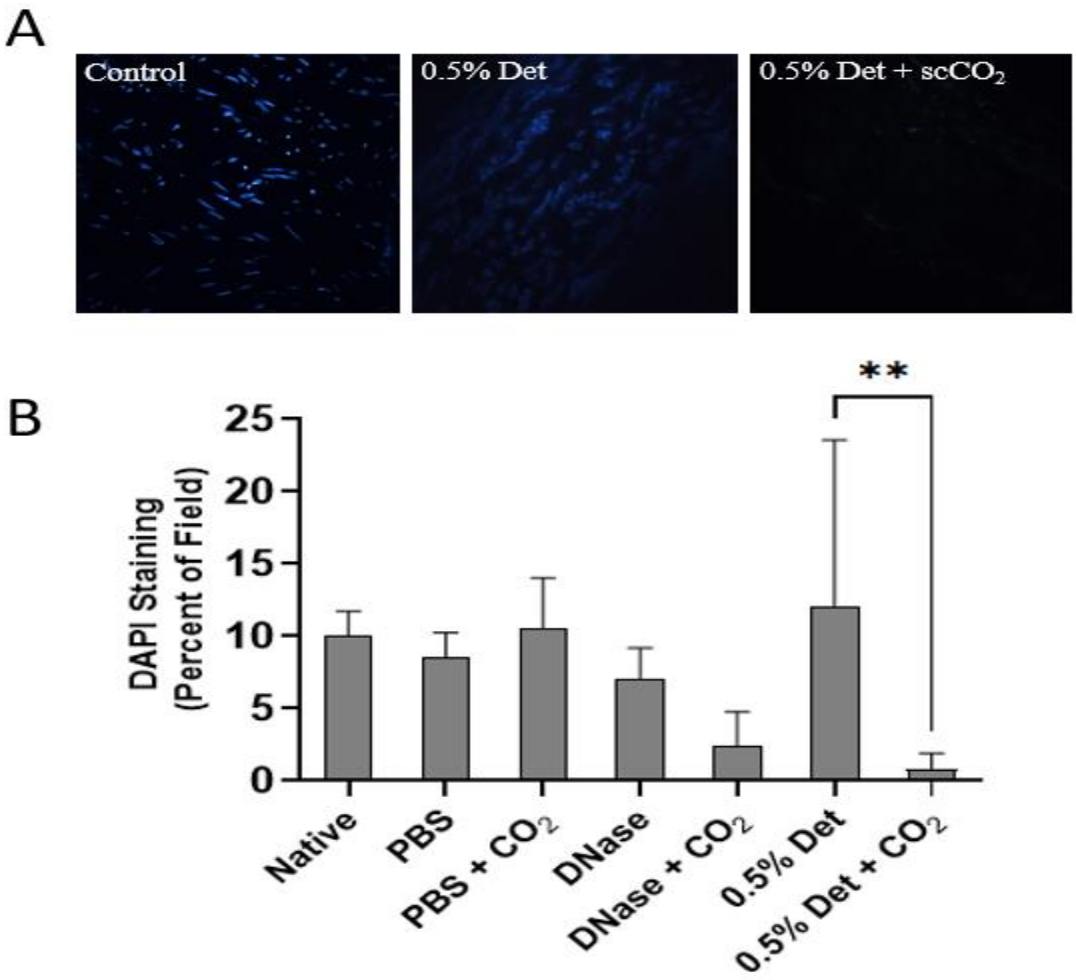

Figure 3.3 – DAPI stain following 2 h of anionic detergent treatment followed by one hour of $scCO_2$ treatment (A). The insets are representative images of DAPI-stained sections of PBS (control), 0.5% detergent-treated, and 0.5% detergent plus $scCO_2$-treated tissues. Area fraction quantification of DAPI-positive pixels (B). Statistical significance between treatments and relative to untreated controls was determined by one-way ANOVA and is indicated by (**) at $p < 0.01$. Mean ± SD, $n = 7$ for each group.

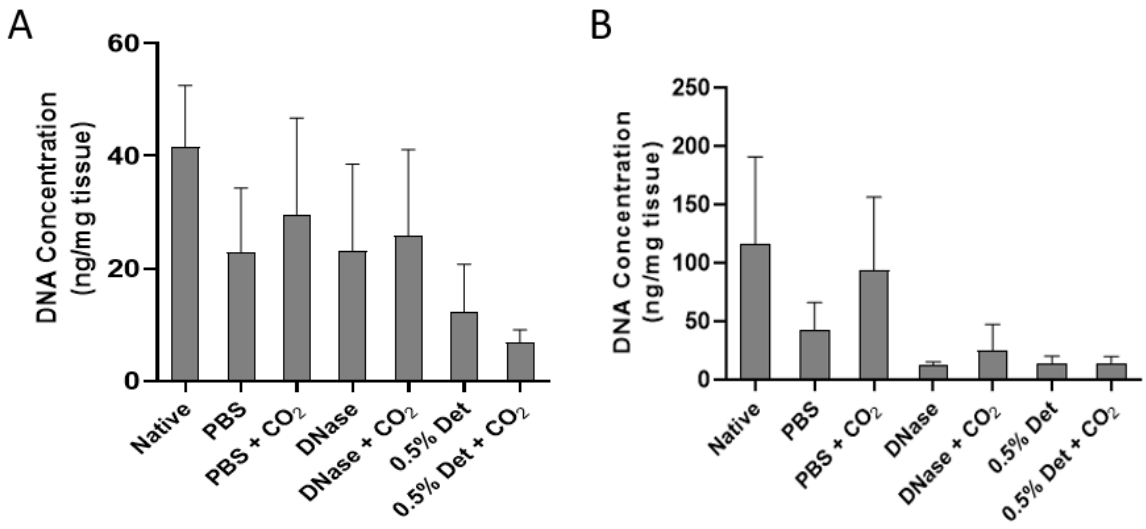

Figure 3.4 – Quantification of DNA content from PicoGreen assays following 24 h (A) and 2 h (B) of anionic detergent treatment plus $scCO_2$ treatment. No statistically significant differences were found following ANOVA analysis. Mean ± SD, n = 18 (A), mean ± SD, n = 7 (B) for each group, respectively.

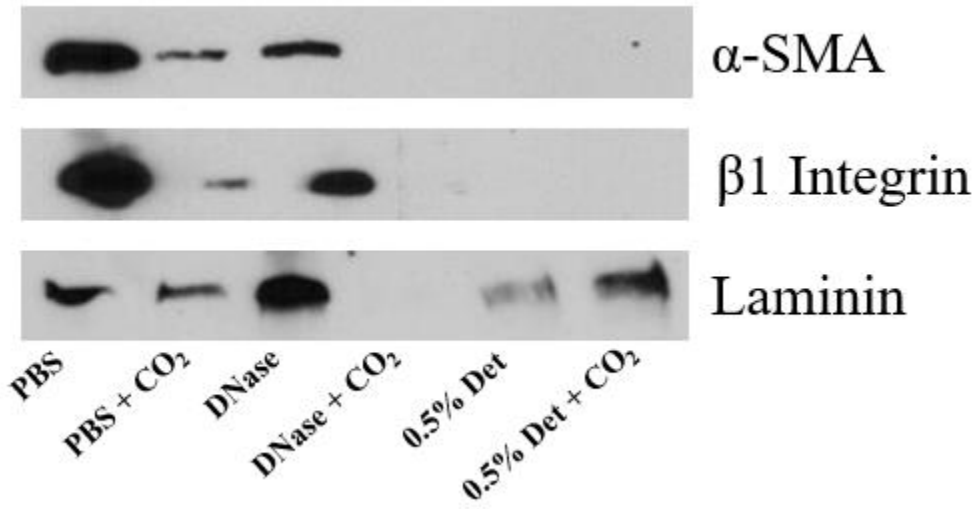

Figure 3.5 – Western blot analysis of representative cytoplasmic (α-smooth muscle actin), cell surface (β1 integrin), and basement membrane (laminin) proteins. Representative images of western blots illustrating the effects of the 2 h SDS/scCO_2 hybrid treatment method. Lanes 1−6 are PBS (untreated control), PBS + CO_2, DNase, DNase + CO_2, 0.5% detergent, and 0.5% detergent + CO_2, respectively.

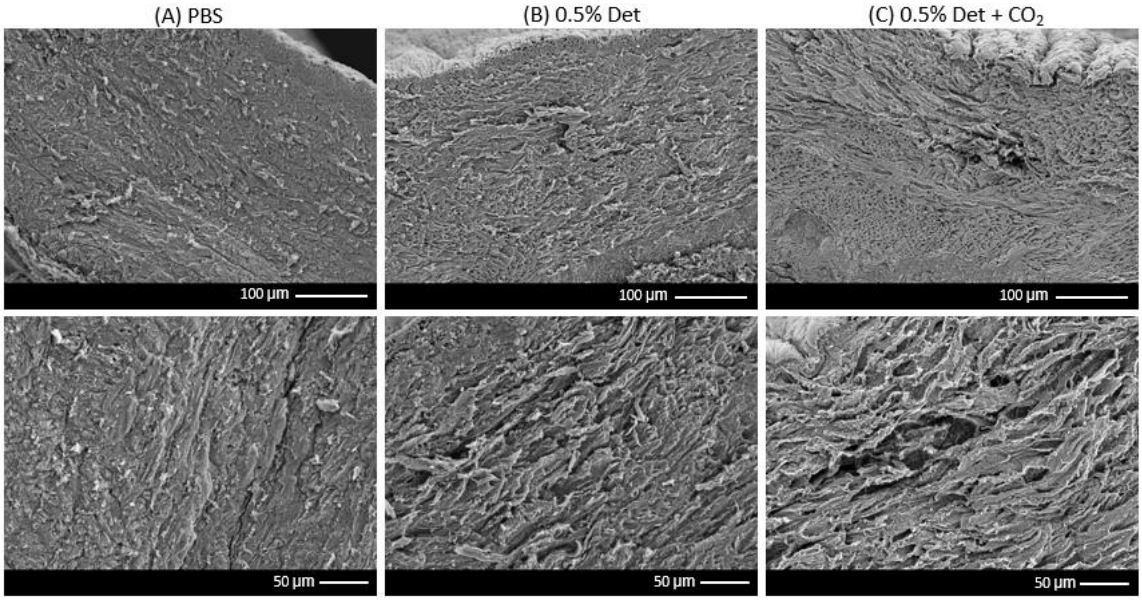

Figure 3.6 – Representative scanning electron microscopic images of (A) control, (B) 2 h 0.5% detergent, and (C) 2 h 0.5% detergent plus $scCO_2$ samples at low and high power magnifications. n = 1 for each group.

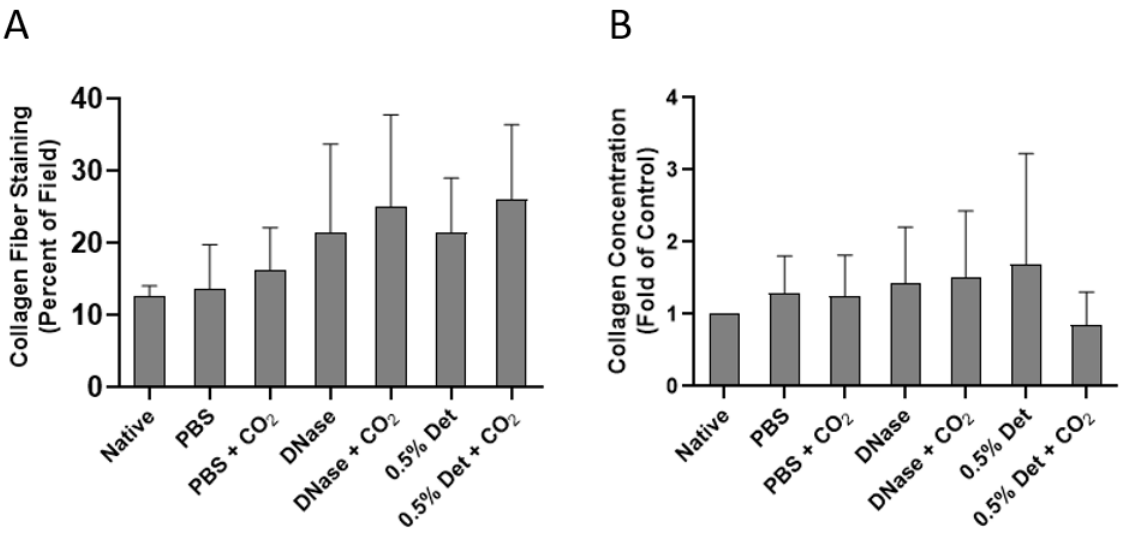

Figure 3.7 – Collagen percent volume quantified by image thresholding of PSR-stained tissue sections after 2 h SDS/scCO2 hybrid treatment (A). Quantification of hydroxyproline concentrations after 2 h SDS/scCO2 hybrid treatment (B). No statistically significant differences were found following ANOVA analysis. Mean ± SD, $n = 7$ for each group.

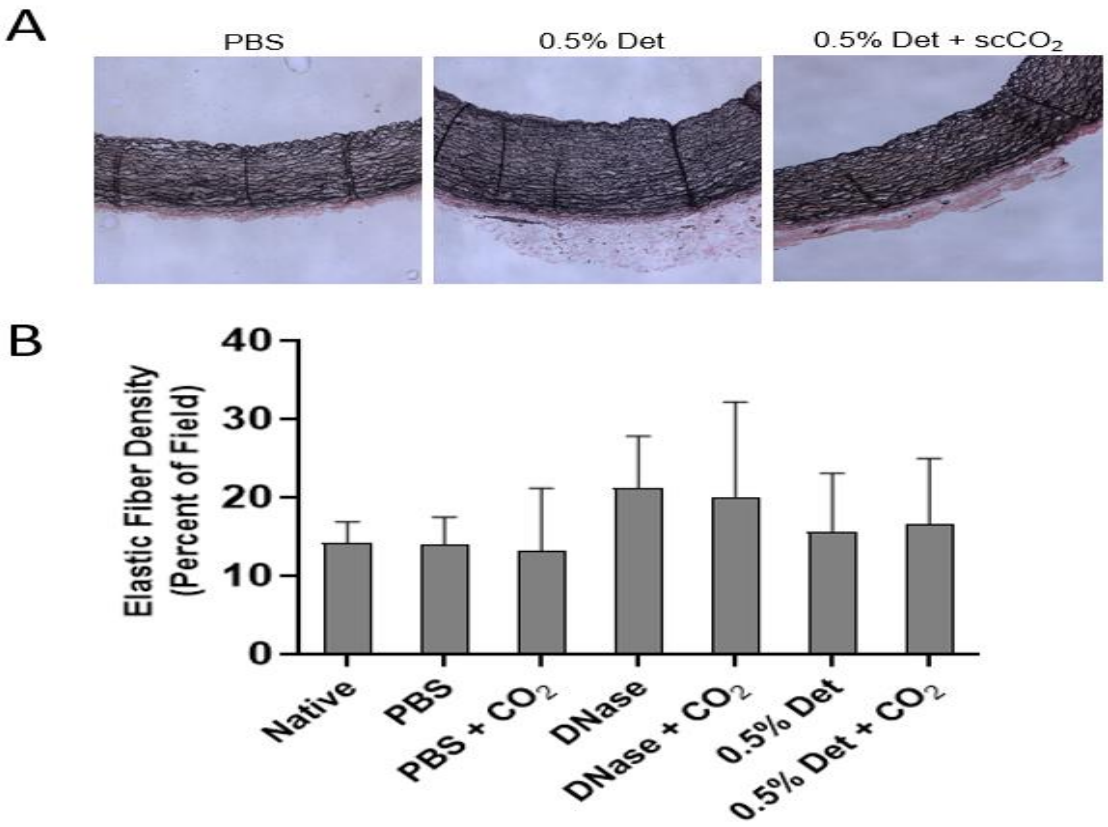

Figure 3.8 – Quantitative analysis of elastic fibers following 2 h SDS/$scCO_2$ hybrid treatment. Representative microscopic images of PBS (control) samples, 0.5% detergent, and 0.5% detergent plus $scCO_2$ following 2 h SDS/$scCO_2$ hybrid treatment (A). Elastic fiber area fraction was quantified from VVG-stained tissue following 2 h SDS/$scCO_2$ hybrid treatment (B). No statistically significant differences were found following ANOVA analysis. Mean ± SD, n = 7 for each group.

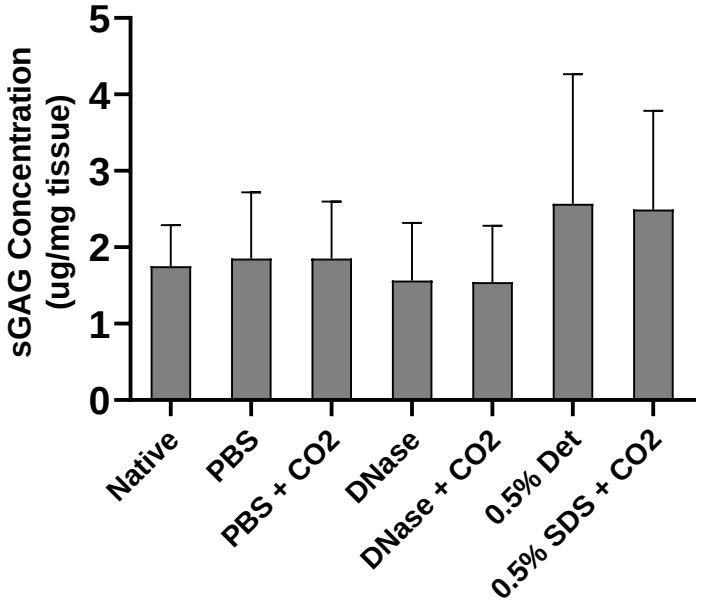

Figure 3.9 – Analysis of dimethylmethylene blue (DMMB) concentrations following 2 h SDS/scCO_2 hybrid treatment. DMMB concentration was indicative of glycosaminoglycan concentration present in all tissue samples. No statistically significant differences were found following ANOVA analysis. Mean ± SD, n = 7 for each group.

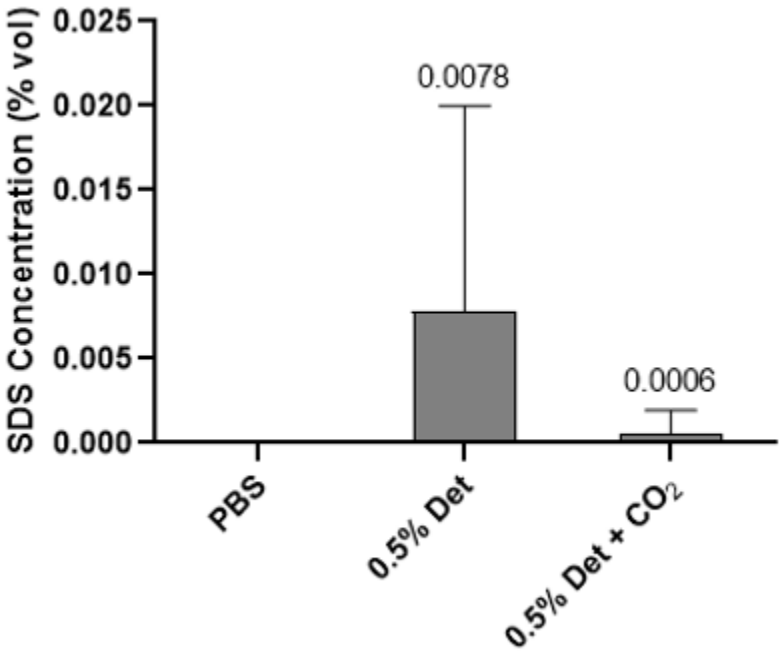

Figure 3.10 – Quantification of residual SDS following treatment after washing with $scCO_2$. 2 h of 0.5% SDS plus 1 hour of $scCO_2$ reduces SDS concentration below the cytotoxic level of 0.002%. No statistically significant differences were found following ANOVA analysis. Mean ± SD, n = 5 for each group.

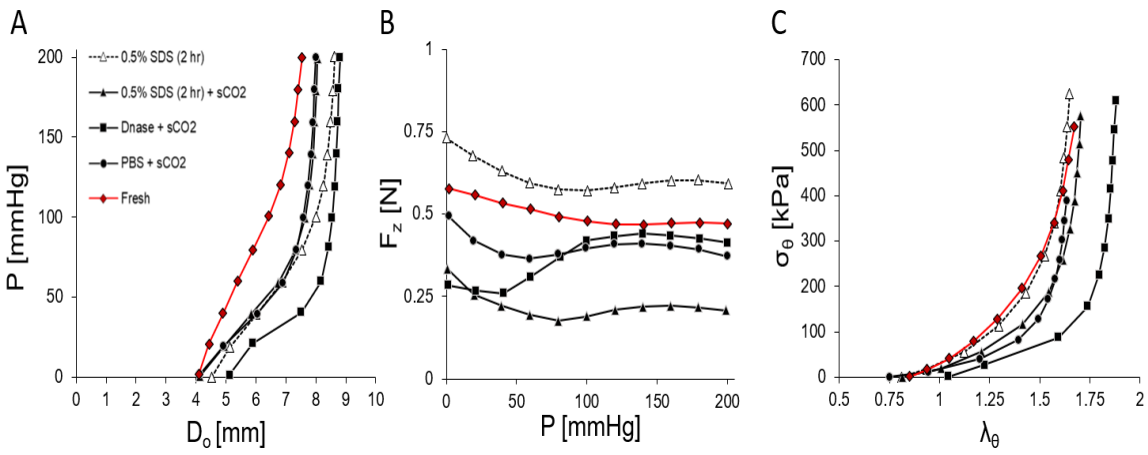

Figure 3.11 – Biaxial mechanical data for fresh and 2 h SDS/scCO$_2$ decellularized porcine ITAs plotted throughout the entire pressure range 0-200 mmHg. (A) Pressure-outer diameter, (B) axial force-pressure, (C) circumferential stress-stretch all plotted at the force-invariant axial stretch (λ_z = 1.45). *n* = 1 for each group.

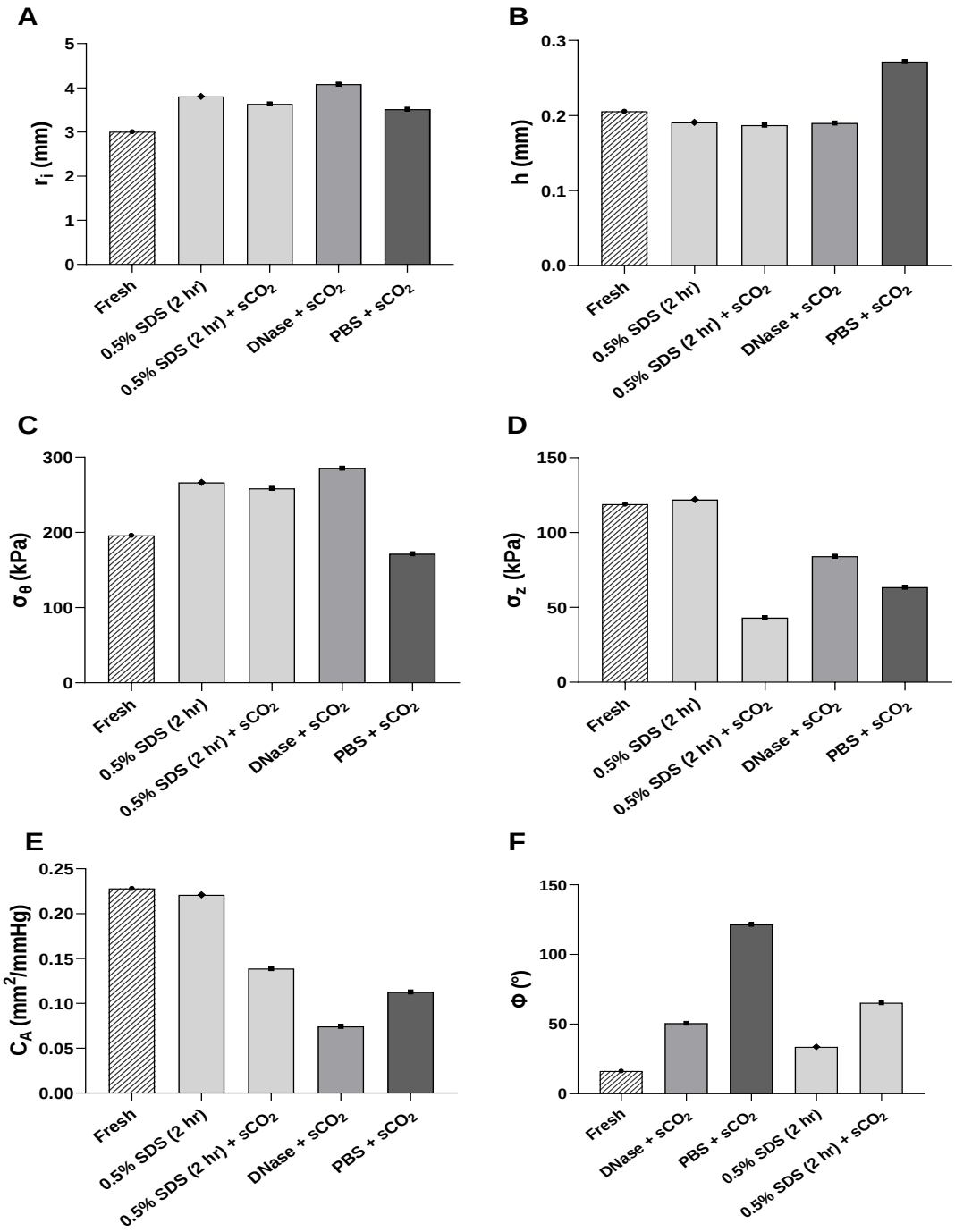

Figure 3.12 – Biaxial mechanical data of fresh and 2 h SDS/scCO$_2$ decellularized porcine ITAs plotted at common loading conditions of 100 mmHg and λ_z = 1.45. (A) Inner radius, (B) thickness, (C) circumferential stress, (D) axial stress, (E) area compliance, and (F) opening angle. n = 1 for each group.

CHAPTER 4

FINAL CONCLUSIONS AND FUTURE DIRECTIONS

Using xenogeneic biomaterials fabricated by human or animal organs/tissues to produce acellular or decellularized extracellular matrix scaffolds (dECM) offers several advantages in the field of tissue engineering (TE). However, while enormous progress has been made in designing safe and effective biomimetic scaffolds, establishing consistent and effective decellularization protocols has proved challenging. These scaffolds can be prepared through a number of decellularization methods, yet innovative approaches are currently being pursued to improve the efficiency of cellular removal, maintenance of native tissue properties, and the safety of xenotransplanted tissues. In general, chemical and enzymatic techniques are mainly responsible for successful decellularization in most protocols to date; however, these protocols must be designed in line with the properties of the target tissue, aiming to preserve specific ECM components and requiring a delicate balance between decellularization efficiency and ECM maintenance. This is difficult, as detergent-based methods tend to disrupt ECM ultrastructure and composition and can ultimately impair tissue functionality. While the literature is extensive regarding detergent-based decellularization methods, a number of shortcomings remain with this approach. $scCO_2$-based decellularization has recently been introduced as a novel and more innovative approach used to address the inadequacies of detergent-based decellularization. Despite the many advantageous properties of $scCO_2$,

less research has been undertaken on its use to fabricate replacement tissues or scaffolds directly from natural biomaterials by decellularization when compared to detergent-based methods. From the small number of studies carried out to date, there is substantial disagreement regarding the ability of $scCO_2$ alone to decellularize tissues. Therefore, the challenge remains in defining broadly acceptable standardized decellularization and characterization procedures for tissue-specific cell removal and dECM fabrication. In the studies presented herein, we have attempted to meet this challenge by evaluating the effects of 1) anionic detergent concentration and duration of treatment and, (2) inclusion of $scCO_2$ on decellularization effectiveness and subsequent structural and mechanical properties of porcine ITAs.

The studies presented in Chapter 2 illustrated that incubation of porcine ITAs for extended periods of time (3 days) and in relatively high concentrations of detergent are required to remove nuclear material most effectively within the porcine ITAs. However, several disadvantages were apparent using this detergent-based protocol including alterations to the tissue composition and structure, relatively lengthy protocol, and residual SDS that will likely compromise recellularization. The results of the study presented in Chapter 2 were then used to develop a more efficient protocol for porcine ITA decellularization utilizing $scCO_2$. As discussed in Chapter 3, the SDS/$scCO_2$ hybrid treatment was tested by assessing the decellularization efficiency and maintenance of tissue-specific ECM components following low concentration SDS pretreatments at two time points with and without $scCO_2$. Similar results were achieved, as both 2 and 24 h detergent treatment plus $scCO_2$ revealed decellularization below the suggested criteria of less than 50 ng of dsDNA per mg of ECM dry weight and was comparable with the DNA

concentration results from the enzyme-detergent method in Chapter 2. Because it was efficient at removing DNA content and the tissue spent less time in detergent as to prevent ECM degradation, the 2 h detergent treatment plus $scCO_2$ was selected as a more optimized protocol moving forward. This produced a time savings of about 22 h compared to the 24 h detergent plus $scCO_2$ treatment and about 5 days compared to the treatment with 1% detergent for 72 h presented in Chapter 2.

A host of assays were used to assess the structural and biochemical properties of the porcine ITAs to determine the extent to which the 2 h detergent treatment plus $scCO_2$ maintained native tissue properties. Future research should include morphometric analyses to quantitatively assess structural changes including tissue porosity and ECM organization more thoroughly, studies to better understand when sGAG tissue content is reduced or lost and how it could be retained during decellularization, assessment of bioactivity, and eventually scaffold testing in animal models.

As mentioned above, global comparison of the ECM composition of decellularized scaffolds and native tissue by proteomic analysis would be advantageous to assess which specific ECM proteins are more susceptible to loss compared to others. Regarding sGAG loss, investigation into the level of acceptable sGAG removal in porcine ITAs should be performed to better characterize the usefulness of individual decellularizing techniques to determine how much sGAG content could be lost without compromising native tissue structure and function. While it is well established that sGAGs are an important component of the ECM, playing roles in embryonic development and ECM assembly and regulation of cell signaling in various physiological and pathological conditions (Lepedda et al., 2021), further investigation toward

delineating the specific roles individual types of sGAGs play within the ECM of the porcine ITA will be necessary to fully understand and elucidate the importance of GAGs within these ITA scaffolds (Sacket et al., 2018). The data presented in Chapter 3 suggests that treatment with 0.5% detergent alone and with $scCO_2$ may retain sGAGs more than other treatments presented in this dissertation; however, this should be investigated more thoroughly. Determining methods to maintain or reintroduce sGAG content within the decellularized scaffolds would be most beneficial. Additionally, the effects of $scCO_2$ on scaffold recellularization could be examined using a perfusion bioreactor system to mimic the in vivo environment more effectively and to assess endothelialization and smooth muscle infiltration using porcine vascular endothelial cells and porcine vascular smooth muscle cells, respectively. A reduction in the basement membrane protein laminin was seen with both the enzyme-detergent treatment (Chapter 2) and the SDS/$scCO_2$ hybrid treatment (Chapter 3) when compared to untreated controls, which could have adverse effects on endothelialization of scaffolds as vascular cells readily adhere to this protein. Because of this, it may also be advantageous to evaluate the effects on endothelialization by altering the intimal surface of the treated scaffolds with laminin. The use of $scCO_2$ for decellularization can be expanded to additional tissues once the SDS/$scCO_2$ hybrid method is better understood in porcine ITAs.

In addition to decellularization, scCO2 has a host of other biomedical applications including the terminal sterilization of sensitive biomaterials (Bernhardt et al., 2015). $scCO_2$ has an established history of use for sterilization in the food, biomedical, and pharmaceutical industries (Dillow et al., 1999; White et al., 2006; Sun et al., 2014). Recently, $scCO_2$ sterilization has been demonstrated on numerous human tissues used for

tissue grafting including tendon and bone, heart valves, and lung matrices (Nichols et al., 2009; Balestrini et al., 2016; Hennessy et al., 2017). A small list of literature suggests that scCO2 could even be used to simultaneously decellularize and sterilize tissue scaffolds (You L, et al., 2018; Uquillas et al., 2021); however, this was not investigated in this dissertation. The possibility of simultaneous decellularization and sterilization or high level disinfection would be huge for the field of tissue engineering. However, the scCO2 technology has points to be improved and further investigation is required regarding ECM sterilization. Yet, if possible, this would greatly improve the efficiency of dECM fabrication by reducing the time it takes to develop such scaffolds even further.

REFERENCES

Ahmed E, Saleh T, Xu M. **Recellularization of native tissue derived acellular scaffolds with mesenchymal stem cells.** *Cell.* 2021; **10**(7):1787.

Ahmed S, Chauhan VM, Ghaemmaghami AM, Aylott JW. **New generation of bioreactors that advance extracellular matrix modeling and tissue engineering.** *Biotechnol Lett.* 2019; **4**(1):1-25.

Angelini GD, Newby AC. **The future of saphenous vein as a coronary artery bypass conduit.** *Eur Heart J.* 1989; **10**(3):273-280.

Badylak SF, Weiss DJ, Caplan A, Macchiarini P. **Engineering whole organs and complex tissues.** *Lancet.* 2012; **379**:943-952.

Balestrini JL, et al. **Sterilization of lung matrices by supercritical carbon dioxide.** *Tissue Eng Part C Methods.* 2016; **22**:260-269.

Baptista PM, Siddiqui MM, Lozier G, Rodriguez SR, Atala A, Soker S. **The use of whole organ decellularization for the generation of a vascularized liver organoid.** *Hepatology.* 2011; **53**:604.

Beckman EJ. **Supercritical and near-critical CO_2 in green chemical synthesis and processing.** *J Supercrit Fluids.* 2004; **28**(2-3):121-191.

Belviso I, Romano V, Sacco AM, Ricci G, et al. **Decellularized human dermal matrix as a biological scaffold for cardiac repair and regeneration.** *Front Bioeng Biotechnol.* 2020;**8**,229.

Bergmeister H, Schreiber C, Grasl C, et al. **Healing characteristics of electrospun polyurethane grafts with various porosities.** *Acta Biomater.* 2013; **9**,6032-40.

Bertolini FM, Morbiato G, Facco P, et al. **Optimization of the supercritical CO_2 pasteurization process for the preservation of high nutritional value of pomegranate juice.** *J Supercrit Fluids.* 2020; **164**:104914.

Böer U, Lohrenz A, Klingenberg M, Pich A, Haverich A, Wilhelmi M. **The effect of detergent-based decellularization procedures on cellular proteins an immunogenicity in equine carotid artery grafts.** *Biomaterials.* 2011; **32**(36):9730-9737.

Brown BN, Freund JM, Han L, et al. **Comparison of three methods for the derivation of a biologic scaffold composed of adipose tissue extracellular matrix.** *Tissue Eng – Part C Methods.* 2011; **17**(4):411-421.

Bruyneel AA, Carr CA. **Ambiguity in the presentation of decellularized tissue composition: the need for standardized approaches.** *Artif Organs*. 2017; **41**(8):778-784.

Cameron A, Davis KB, Green G, Schaff HV. **Coronary bypass surgery with internal-thoracic-artery grafts – effects on survival over a 15-year period.** *N Engl J Med.* 1996; **334**(4):216-219.

Campinoti S, Gjinovci A, Ragazzini R, et al. **Reconstitution of a functional human thymus by postnatal stromal progenitor cells and natural whole-organ scaffolds.** *Nat Commun.* 2020; **11**, 6372.

Carlès P. **A brief review of the thermophysical properties of supercritical fluids.** *J Supercrit Fluids.* 2010; **53**,2-11.

Cartmell JS, Dunn MG. **Effect of chemical treatments on tendon cellularity and mechanical properties.** *J Biomed Mater Res.* 2000; **49**,134-140.

Cartmell JS, Dunn MG. **Development of cell-seeded patellar tendon allografts for anterior cruciate ligament construction.** *Tissue Eng.* 2004; **10**(7-8):1065-1075.

Casali DM, Handleton RM, Shazly T, Matthews MA. **A novel supercritical CO_2-based decellularization method for maintaining scaffold hydration and mechanical properties.** *J Supercrit Fluids.* 2018; **131**: 72-81.

Celikkin N, Rinoldi C, Costantini M, Trobetta M, Rainer A, Święszkowski W. **Naturally derived proteins and glycosaminoglycan scaffolds for tissue engineering applications**. *Mater Sci Eng C.* 2017; **78**:1277-1299.

Chard RB, Johnson DC, Nunn GR. Cartmill TB. **Aorta-coronary bypass grafting with polytetrafluoroethylene conduits. Early and late outcome in eight patients.** *J Thorac Cardiovasc Surg.* 1987; **94**,132-134.

Chen SJ, Li JX, Dong PQ. **Utilization of pulsatile flow to decellularize the human umbilical arteries to make small-caliber blood vessel scaffolds.** *Acta Cardiol Sin.* 2013; **29**(5):451-456.

Cheng CW, Solorio LD, Alsberg E. **Decellularized tissue and cell-derived extracellular matrices as scaffolds for orthopaedic tissue engineering.** *Biotecnol Adv.* 2014; **32**(2):462-484.

Conte MS. **Critical appraisal of surgical revascularization for critical limb ischemia.** *J Vasc Surg.* 2013; **57**, 8S.

Conte MS. **The ideal small arterial substitute a search for the Holy Grail?** *FASEB J.* 1998; **12**:43-45.

Crampon C, Boutin O, Badens E. **Supercritical carbon dioxide extraction of molecules of interest from microalgae and seaweeds.** *Ind Eng Chem Res.* 2011; **50**(15):8941-8953.

Crapo PM, Gilbert TW, Badylak SF. **An overview of tissue and whole organ decellularization processes.** *Biomaterials.* 2011; **32**(12):3233-3243.

Cross LM, Thakur A, Jalili NA, Detamore M, Gahawar AK. **Nanoengineered biomaterials for repair and regeneration of orthopedic tissue interfaces.** *Acta Biomater.* 2016; **42**:2-17.

Davies OR, Lewis AL, Whitaker MJ, Tai H, Shakesheff KM, Howdle SM. **Applications of supercritical CO_2 in the fabrication of polymer systems for drug delivery and tissue engineering.** *Adv Drug Deliv Rev.* 2008; **60**(3):373-387.

Desai M, Seifalian AM, Hamilton G. **Role of prosthetic conduits in coronary artery bypass grafting.** *European Journal of Cardio-Thoracic Surgery.* 2011; **40**(2):394-398.

Dillow AK, Dehghani F, Hrkach JS, Foster NR, Langer R. **Bacterial inactivation by using near- and supercritical carbon dioxide.** *PNAS.* 1999; **96**:10344-10348.

Donati I, Benincasa M, Foulc MP, Turco G, et al. **Terminal sterilization of BisGMA-TEGDMA thermoset materials and their bioactive surfaces by supercritical CO_2.** *Biomacromolecules.* 2012; **13**(4):1152-1160.

Duarte MM, Ribeiro N, Silva IV, et al. **Fast decellularization process using supercritical carbon dioxide for trabecular bone.** *J Supercrit Fluids.* 2021; **172**, 105194.

Duarte MM, Silva IV, Eisenhut AR, et al. **Contributions of supercritical fluid technology for advancing decellularization and postprocessing of viable biological materials.** *Mater Horiz.* 2022; **9**,864-891.

Elder BD, Kim DH, Athanasiou KA. **Developing an articular cartilage decellularization process toward fact joint cartilage replacement.** *Neurosurgery.* 2010; **66**,722-727.

Ellis JL, Titone JC, Tomasko DL, Annabi N, Dehghani F. **Supercritical CO_2 sterilization of ultra-high molecular weight polyethylene.** *J Supercrit Fluids.* **52**(2):235-240.

Faggioli M, Moro A, Butt S, Todesco M, Sandrin D, et al. **A new decellularization protocol of porcine aortic valves using tergitol to characterize the scaffold with the biocompatibility profile using human bone marrow mesenchymal stem cells.** *Polymers.* 2022; **14**(6),1226.

Faulk DM, Badylak SF. **Chapter 8 – Natural biomaterials for regenerative medicine applications.** *Regenerative Medicine Applications in Organ Transplantation.* 2014; 101-112.

Faulk DM, Carruthers CA, Warner HJ, et al. **The effect of detergents on the basement membrane complex of a biologic scaffold material.** *Acta Biomater.* 2014; **10**(1):183-193.

Fernández-Pérez J, Ahearne M. **The impact of decellularization methods on extracellular matrix derived hydrogels.** *Scientific Reports.* 2019; **9**,14933.

Fleury C, Savoire R, Harscoat-Schiavo C, Hadj-Sassi A, Subra-Paternault P. **Optimization of supercritical CO_2 process to pasteurize dietary supplement: influencing factors and CO_2 transfer approach.** *J Supercrit Fluids.* 2018; **141**:240-251.

Floren M, Spilimbergo S, Motta A, Migliaresi C: **Porous poly(D,L-lactic acid) foams with tunable structure and mechanical anisotropy prepared by supercritical carbon dioxide.** *J Biomed Mat Res Part B – Appl Biomater.* 2011; **99B**(2):338-349.

Flynn LE. **The use of decellularized adipose tissue to provide an inductive microenvironment for the adipogenic differentiation of human adipose-derived stem cells.** *Biomaterials.* 2010; **31**:4715-4724.

Forouzesh F, Rabbani M, Bonakdar S. **A comparison between ultrasonic bath and direct sonicator on osteochondral tissue decellularization.** *J Med Signals Sens.* **9**(4),227-233.

Funamoto S, Nam K, Kimura T, et al. **The high use of high-hydrostatic pressure treatment to decellularize blood vessels.** *Biomaterials.* 2010; **31**(13):3590-3595.

Garcia-Gonzalez CA, Concheiro A, Alvarez-Lorenzo C. **Processing of material for regenerative medicine using supercritical fluid technology.** *Bioconjug Chem.* 2015; **26**(7):1159-1171.

Gershlak JR, Hernandez S, Fontana G, et al. **Crossing kingdoms: using decellularized plants as perfusable tissue engineering scaffolds.** *Biomaterials.* 2017; **125**, 13-22.

Gilbert TW, Sellaro TL, Badylak SF. **Decellularization of tissues and organs.** *Biomaterials.* 2006; **27**(19):3675-3683.

Gilpin A, Yang Y. **Decellularization strategies for regenerative medicine: from processing techniques to applications.** *Biomed Res Int.* 2017; **2017**:9831534.

Go A, Mozaffarian D, Roger V. **Executive summary: heart disease and stroke statistics – 2014 update: a report of the American Heart Association.** *Circulation.* 2014; **129**:399-410.

Gratzer PF, Harrison RD, Woods T. **Matrix alteration and not residual sodium dodecyl sulfate cytotoxicity affects the cellular repopulation of a decellularized matrix.** *Tissue Eng.* 2006; **12**(10):2975-2983.

Gregory E, Baek IH, Ala-Kokko N, et al. **Peripheral nerve decellularization for in vitro extracellular matrix hydrogel use: a comparative study.** *ACS Biomater Sci Eng.* 2022; **8**(6):2574-2588.

Guler S, Aslan B, Hosseinian P, Aydin HM. **Supercritical carbon dioxide-assisted decellularization of aorta and cornea.** *Tissue Eng Part C: Methods.* 2017; **23**(9):540-547.

Hadinata IE, Hayward PA, Hare DL, et al. **Choice of conduit for the right coronary system: 8-year analysis of radial artery patency and clinical outcomes trial.** *Ann Thorac Surg.* 2009; **88**,1404-1409.

Hall A, Brilakis ES. **Saphenous vein graft failure: seeing the bigger picture.** *J Thorac Dis.* 2019; **11**:S399-403.

Harris AF, Lacombe J, Liyange S, et al. **Supercritical carbon dioxide decellularization of plant material to generate 3D biocompatible scaffolds.** *Sci Rep.* 2021; **11**, 3643.

Hashemi J, Pasalar P, Soleimani M, et al. **Decellularized pancreas matrix scaffolds for tissue engineering using ductal or arterial catheterization.** *Cells Tissues Organs.* 2018; **205**:72.

Hazwani A, Sha'Ban M, Azhim A. **Characterization and in vivo study of decellularized aortic scaffolds using closed sonication system.** *Organogenesis.* 2019; **15**(4):120-136.

Hennessy RS, et al. **Supercritical carbon-dioxide based sterilization of decellularized heart valves.** *JACC: Basic to Translational Science.* 2017; **2**:71-84.

Hillebrandt KH, Everwien H, Haep N, Keshi E, Pratschke J, Sauer IM. **Strategies based on organ decellularization and recellularization.** *Transplant International.* 2019; **32**:571-585.

Hiob MA, She S, Muiznieks LD, Weiss AS. **Biomaterials and modifications in the development of small-diameter vascular grafts.** *ACS Biomater Sci Eng.* 2017; **3**,712-723.

Hoenig MR, Campbell GR, Rolfe BE, et al. **Tissue-engineered blood vessels: alternative to autologous grafts?** *Arterioscler Thromb Vasc Biol.* 2005; **25**,1128-1134.

Hsieh DJ, Srinivasan P, Yen KC, Yeh YC, Chen YJ, Wang HC, Tarng YW. **Protocols for the preparation and characterization of decellularized tissue and organ scaffolds for tissue engineering.** *BioTechniques.* 2020; **70**(2):1-9.

Huang YH, et al. **Preparation of acellular scaffold for corneal tissue engineering by supercritical carbon dioxide extraction technology.** *Acta Biomater.* 2017; **58**:238-243.

Hwang J, San BH, Turner NJ, et al. **Molecular assessment of collagen denaturation in decellularized tissues using a collagen hybridizing peptide.** *Acta Biomater.* 2017; **53**:268-278.

Ikada Y. **Challenges in tissue engineering.** *J R Soc Interface.* 2006; **3**(10):589-601.

Jones RS, Chang PH, Perahia T, et al. **Design and fabrication of a three-dimensional in vitro model of vascular stenosis.** *Microsc Micro-anal.* 2016; **22**(S3):1766-1767.

Kannan RY, Salacinski HJ, Butler PE, et al. **Current status of prosthetic bypass grafts: A review.** *J Biomed Mater Res B Appli Biomater.* 2005; **74**,570-581.

Keane TJ, Badylak SF. **The hose response to allogenic and xenogeneic biological scaffold materials.** *J Tissue Eng Regen Med.* 2015; **9**, 504-511.

Keane TJ, Swinehart IT, Badylak SF. **Methods of tissue decellularization used for preparation of biologic scaffolds and *in vivo* relevance.** *Methods.* 2015; **84**(2015):25-34.

Keane TJ, Londono R, Turner NJ, Badylak SF. **Consequences of ineffective decellularization of biologic scaffolds on the host response.** *Biomaterials.* 2012; **33**(6):1771-1781.

Kim FY, Marhefka G, Ruggiero NJ, Adams S, Whellan DJ. **Saphenous vein graft disease: review of pathophysiology, prevention, and treatment.** *Cardiol Rev.* 2013; **21**(2):101-109.

Kitano K, Schwartz DM, Zhou H, et al. **Bioengineering of functional human induced pluripotent stem cell-derived intestinal grafts.** *Nat Commun.* 2017; **8**:765.

Klinkert P, Post PN, Breslau PJ, van Bockel JH. **Saphenous vein versus PTFE for above-knee femoropopliteal bypass.** *Eur J Vasc Endovasc Surg.* 2004; **27**(4):357-362.

Kostelnik CJ, Crouse KJ, Carver W, Eberth JF. **Longitudinal histomechanical heterogeneity of the internal thoracic artery.** *J Mech Behav Biomed Mater.* 2020; **2021**(116):104314.

Kostelnik CJ, Hohn J, Escoto-Diaz CE, et al. **Small-diameter artery decellularization: Effects of anionic detergent concentration and treatment duration on porcine internal thoracic arteries.** *J Biomed Mater Res.* 2021; 1-13.

Lamm P, Juchem G, Milz S, Schuffenhauer M, Reichart B. **Autologous endothelialized vein allograft: a solution in the search for small-caliber grafts in coronary artery bypass graft operations.** *Circulation.* 2001; **104**[suppl I]:I-108-I-114.

Lehr EJ, Rayat GR, Chiu B, Churchill T, McGann LE, Coe JY, et al. **Decellularization reduces immunogenicity of sheep pulmonary artery vascular patches.** *J Thorac Cardiovasc Surg.* 2010; **141**(4):1056-1062.

Lepedda AJ, Nieddu G, Formato M, Baker MB, Fernandez-Perez J, Moroni L. **Glycosaminoglycans: from vascular physiology to tissue engineering applications.** *Front. Chem.* 2021: **9**:680836.

Li S, Sengupta D, Chien S. **Vascular tissue engineering: from in vitro to in situ.** *Wiley Interdiscip Rev Syst Biol Med.* 2014; **6**(1):61-76.

Liao J, Joyce EM, Sacks MS. **Effects of decellularization on the mechanical and structural properties of the porcine aortic valve leaflet.** *Biomaterials.* 2008; **29**(8):1065-1074.

Lin CH, Hsia K, Su CH, Chen CC, Yeh CC, Ma H, Lu JH. **Sonication-assisted method for decellularization of human umbilical artery for small-caliber vascular tissue engineering.** *Polymers (Basel).* 2021; **13**(11):1699.

Liu X, Li N, Gong D, Xia C, Xu Z. **Comparison of detergent-based decellularization protocols for the removal of antigenic cellular components in porcine aortic valve.** *Xenotransplantation.* 2018; **25**(2):1-13.

Maghsoudlou P, Totonelli G, Loukogeorgakis SP, Eaton S, De Coppi P. **A decellularization methodology for the production of a natural acellular intestinal matrix.** *J Vis Exp.* 2013; **80**:1-6.

Mahdavi SS, Abdekhodaie MJ. **Bioengineering approaches for corneal regenerative medicine.** *Tissue Eng Regen Med.* 2020.

Mallis P, Chachlaki P, Katsimpoulas M, et al. **Optimization of decellularization procedure in rat esophagus for possible development of tissue engineered construct.** *Bioengineering.* 2019; **6**,3.

McBane JE, Sharifpoor S, Labow RS, et al. **Tissue-engineering a small diameter vessel substitute: engineering constructs with select biomaterials and cells.** *Curr Vasc Pharmacol.* 2012; **10**,347-360.

McFetridge PS, Daniel JW, Bodamyali T, Horrocks M, Chaudhuri JB. **Preparation of porcine carotid arteries for vascular tissue engineering applications.** *J Biomed Mater Res Part A.* 2004; **70**,224-234.

McHugh MA, Krukonis VJ. **Supercritical fluid extraction: principles and practice.** Stoneham, Mass.: Butterworth; 1994.

Mehrali M, Thakur A, Pennisi CP, et al. **Nanoreinforced hydrogels for tissue engineering: biomaterials that are compatible with load-bearing and electroactive tissues.** *Adv Mater.* 2017; **29**(8):1603612.

Mendibil U, Ruiz-Hernandez R, Retegi-Carrion S, et al. **Tissue-specific decellularization methods: rationale and strategies to achieve regenerative compounds.** *Int J Mol Sci.* 2020; **21**, 5447.

Meyer, M. **Processing of collagen based biomaterials and the resulting materials properties.** *Biomed Eng OnLine.* 2019; **18**,24.

Mikos AG, McIntire LV, Anderson JM, Babensee JE. **Host response to tissue engineered devices.** *Adv Drug Deliv Rev.* 1998; **33**(1-2):111-139.

Moffat D, Ye K, Jin S. **Decellularization for the retention of tissue niches.** *J Tissue Eng.* 2022; **13**, 20417314221101151.

Moghadas BK, Azadi M. **Fabrication of nanocomposite foam by supercritical CO_2 technique for application in tissue engineering.** *J Tis Mat.* 2019; **2**(1):23-32.

Mohammadi MS, Buchen JT, Pasquina PF, Nikalson LE, Alvarez LM, Jariwala SH. **Critical considerations for regeneration of vascularized composite tissues.** *Tissue Engineering Part B: Reviews.* 2021; **27**(4):366-381.

Molino A, Larocca V, Di Sanzo G, Martino M, Casella P, Marino T, Karatza D, Musmarra D. **Extraction of bioactive compounds using supercritical carbon dioxide.** *Molecules.* 2019; **24**(4):782.

Moroni F, Mirabella T. **Decellularized matrices for cardiovascular tissue engineering.** *Am J Stem Cells.* 2014; **3**(1):1-20.

Nakamura N, Kimura T, Kishida A. **Overview of the development, applications, and future perspectives of decellularized tissues and organs.** 2017; **3**(7):1236-1244.

Nazari M, Kurdi M, Heerklotz H. **Classifying surfactants with respect to their effect on lipid membrane order.** *Biophys J.* 2012; **102**(3):498-506.

Neishabouri A, Khaboushan AS, Daghigh F, Kajbafzadeh AM, Zolbin MM. **Decellularization in tissue engineering and regenerative medicine: evaluation, modification, and application methods.** *Front Bioeng Biotechnol.* 2022; **10**:805299.

Nichols A, Burns DC, Christopher R. **Studies on the sterilization of human bone and tendon musculoskeletal allograft tissue using supercritical carbon dioxide.** *J Orthopaedics.* 2009; **6**.

Ott HC, Clippinger B, Conrad C, et al. **Regeneration and orthotopic transplantation of bioartificial lung.** *Nat Med.* 2010; **16**:927.

Ott HC, Matthiesen TS, Goh SK, et al. **Perfusion-decellularized matrix: using nature's platform to engineer a bioartificial heart.** *Nat Med.* 2008; **14**:213.

Ozeki M, Narita Y, Kagami H, Ohmiya N, Itoh A, Hirooka Y, et al. **Evaluation of decellularized esophagus as a scaffold for cultured esophageal epithelial cells.** *J Biomed Mater Res A.* 2006;**79**(4):771-778.

Parang P, Arora R. **Coronary vein graft disease: pathogenesis and prevention.** *Can J Cardiol.* 2009; **25**(92):e57-e62.

Park KM, Hussein KH, Hong SH, et al. **Decellularized liver extracellular matrix as promising tools for transplantable bioengineered liver promotes hepatic lineage commitments of induce pluripotent stem cells.** *Tissue Eng Part A.* 2016; **22**:449.

Partington L, Mordan NJ, Mason C, et al. **Biochemical changes caused by decellularization may compromise mechanical integrity of tracheal scaffolds.** *Acta Biomater.* 2013; **9**(2):5251-5261.

Pawan KC, Hong Y, Zhang G. **Cardiac tissue-derived extracellular matrix scaffolds for myocardial repair: advantages and challenges.** *Regenerative Biomaterials.* 2019; **6**(4):185-199.

Pellegata AF, Asnaghi MA, Stefani I, et al. **Detergent-enzymatic decellularization of swine blood vessels: insight on mechanical properties for vascular tissue engineering.** *Biomed Res Int.* 2013; **2013**:918753.

Prim DA, Zhou B, Hartstone-Rose A, Uline M et al. **A mechanical argument for the differential performance of coronary artery grafts.** *J Mech Behav Biomed Mater.* 2016; **54**:93-105.

Pu L, Wu J, Pan X et al. **Determining the optimal protocol for preparing an acellular scaffold of tissue engineered small-diameter blood vessels.** *J Biomed Mater Res – Part B Appl Biomater.* 2018; **106**(2):619-631.

Rabbani M, Zakian N, Alimoradi N. **Contributions of physical methods in decellularization of animal tissues.** *J Med Signals Sens.* 2021; **11**(1):1-11.

Raman R, Sasisekharan V, Sasisekharan R. **Structural insights into biological roles of protein-glycosaminoglycan interactions.** *Chem Biol.* 2005; **12**(3):267-277.

Ren H, Shi X, Tao L, Xiao J, Han B, Zhang Y, Yuan X, Ding Y. **Evaluation of two decellularization methods in the development of a whole-organ decellularized rat liver scaffold.** *Liver International.* 2013; **33**(3):448-458.

Ross EA, Williams MJ, Hamazaki T, et al. **Embryonic stem cells proliferate and differentiate when seeded into kidney scaffolds.** *J Am Soc Nephrol.* 2009; **20**:2338.

Salarian M, Zu WZ, Wang Z, Sham TK, Carpenter PA. **Hydroxyapatite-TiO_2-based nanocomposites synthesized in supercritical CO_2 for bone tissue engineering: physical and mechanical properties.** *ACS Appl Mater Interfaces.* 2014; **6**: 16918-16931.

Santos-Rosales V, Magariños B, Alvarez-Lorenzo C, García-González CA. **Combined sterilization and fabrication of drug-loaded scaffolds using supercritical CO_2 technology.** *Int J Pharmaceutics.* 2022; **612**:121362.

Sawada K, Terada D, Yamaoka T, Kitamura S, Fujisato T. **Cell removal with supercritical carbon dioxide for acellular artificial tissue.** *J Chem Tech and Biotech.* 2008; **83**(6)L943-949.

Seddon AM, Curnow P, Booth PJ. **Membrane proteins, lipids, and detergents: not just a soap opera.** *Biochemica et Biophysica Acta (BBA).* 2004; **1666**(1-2):105-117

Seifu DG, Purnama A, Mequanint K, Mantovani D. **Small-diameter vascular tissue engineering.** *Nat Rev Cardiol.* 2013; **10**,410-421.

Seo Y, Jung Y, Kim SH. **Decellularized heart ECM hydrogel using supercritical carbon dioxide for improved angiogenesis.** *Acta Biomater.* 2018; **67**:270-281.

Shah PJ, Bui K, Blackmore S, Gordon I, Hare DL, Fuller J, Seevanayagam S, Buxton BF. **Has the in situ internal thoracic artery been overlooked? An angiographic study of the radial artery, internal thoracic arteries, and saphenous vein graft patencies in symptomatic patients.** *Eur J Cardio-Thorac Surg.* 2005; **27**,870-875.

Sherifi I, Bachy M, Laumonier T, Petite H, Hannouche D. **Use of supercritical carbon dioxide technology for fabricating a tissue engineering scaffold for anterior cruciate ligament repair.** *Sci Rep.* 2020; **10**:14030.

Simsa R. Padma AM, Heher P, et al. **Systematic *in vitro* comparison of decellularization protocols for blood vessels.** *PLoS One.* 2018; **13**(12):e0209269.

Sudbrack TP, Archilha NL, Itri R, Riske KA. **Observing the solubilization of lipid bilayers by detergents with optical microscopy of GUVs.** *J Phys Chem B.* 2011; **115**(2):269-277.

Sulaiman NS, Bond AR, Ascione R, et al. **Effective decellularization of human saphenous veins for biocompatible arterial tissue engineering applications: bench optimization and feasibility in vivo testing.** *J Tissue Engineering.* 2021; **12**.

Sun Y. **Supercritical fluid particle design for poorly water-soluble drugs (review).** *Curr Pharm Des.* 2014; **20**:349-368.

Tai HY, Mather ML, Howard D, Wang WX, White LJ, Crowe JA, Morgan SP, Chandra A, Williams DJ, Howdle SM, et al. **Control of pore size and structure of tissue engineering scaffolds produced by supercritical fluid processing.** *European Cells & Materials.* 2007; **14**:64-76.

Tapias LF, Ott HC. **Decellularized scaffolds as a platform for bioengineered organs.** *Curr Opin Organ Transplant.* 2014; **19**(2): 145-152.

Thom T, Haase N, Rosamond W, et al. American Heart Association Statistics, C.; Stroke Statistics, S. **Heart disease and stroke statistics – 2006 update: A report from the American Heart Association Statistics Committee and Stroke Statistics Subcommittee.** *Circulation.* 2006; **113**,e85-e151.

Topuz B, Günal G, Guler S, Aydin HM. **Chapter 4 – Use of supercritical CO_2 in soft tissue decellularization.** *Methods in Cell Biology.* 2020; **157**,49-79.

Tran HLB, Doan VN, To QM, et al. **Decellularization of bone tissue.** *Adv Exp Med Biol.* 2021; **1345**:225-239.

Uhl FE, Zhang F, Pouliot RA, at al. **Functional role of glycosaminoglycans in decellularized lung extracellular matrix.** *Acta Biomater.* 2019; **102**(2020):231-246.

Uquillas JA, Spierings J, van der Lande A, et al. **An off-the-shelf decellularized and sterilized human bone-ACL-bone allograft for anterior cruciate ligament reconstruction.** *J Mech Behav Biomed Mater.* 2022; **135**:105452.

Vedadghhavami A, Minooei F, Mohammadi MH, et al. **Manufacturing of hydrogel biomaterials with controlled mechanical properties for tissue engineering applications.** *Acta Biomater.* 2017; **62**(July):42-63.

Yang B, Zhang Y, Zhou L, Sun Z, Zheng J, Chen Y, et al. **Development of a porcine bladder acellular matrix with well-preserved extracellular bioactive factors for tissue engineering.** *Tissue Eng Part C Methods.* 2010; **16**(5):1201-1211.

You L, Weikang X, Lifeng Y, et al. **In vivo immunogenicity of bovine bone removed by a novel decellularization protocol based on supercritical carbon dioxide.** *Artificial Cells, Nanomedicine, and Biotechnology.* 2018; **46**(sup2): 334-344.

Yu Y, Alkhawaji A, Ding Y, Mei J. **Decellularized matrices for cardiovascular tissue engineering.** *Decellularized Scaffolds in Regenerative Medicine.* 2016; **7**:36-58683.

Waldrop FS, Puchtler H, Meloan SN, Younker TD. **Histochemical investigations of different types of collagen.** *Acta Histochem Suppl.* 1980; **21**,23-31.

Wang X, Lin P, Yao Q, Chen C. **Development of small-diameter vascular grafts.** *World J Surg.* 2007; **31**,682-689.

White A, Burns D, Christensen TW. **Effective terminal sterilization using supercritical carbon dioxide.** *J Biotechnol.* 2006; **123**(4):504-515.

White MT, Bianchi G, Chai L, Tassou SA, Sayma AI. **Review of supercritical CO_2 technologies and systems for power generation.** *Applied Thermal Engineering.* 2021; **185**, 116447.

Wiles K, Fishman JM, De Coppi P, Birchall MA. **The hose immune response to tissue-engineered organs: current problems and future directions.** *Tissue Eng Part B Rev.* 2016; **22**(3):208-19.

Williams C, Liao J, Joyce EM, et al. **Altered structural and mechanical properties in decellularized rabbit carotid arteries.** *Acta Biomater.* 2009; **5**(4):993-1005.

Wolf MT, Daly KA, Brennan-Pierce EP, et al. **A hydrogel derived from decellularized dermal extracellular matrix.** *Biomaterials.* 2012; **33**, 7028-7038.

Wong ML, Griffiths LG. **Immunogenicity in xenogeneic scaffold generation: antigen removal vs. decellularization.** *Acta Biomater. 2014;* **10**(5):1806-1816.

Woods T, Gratzer PF. **Effectiveness of three extraction techniques in the development of a decellularized bone-anterior cruciate ligament-bone graft.** *Biomaterials.* 2005; **26**, 7339-7349.

Yu Y, Alkhawaji A, Ding Y, Mei J. **Decellularized scaffolds in regenerative medicine.** *Decellularized Scaffolds in Regenerative Medicine Oncotarget.* 2016; 7(36): 58761-58683.

Zhang X, Chen X, Hong H, Hu R, Liu J, Liu C. **Decellularized extracellular matrix scaffolds: recent trends and emerging strategies in tissue engineering.** *Bioact Mater*. 2021; **10**:15-31.

Zhou B, Prim DA, Romito EJ, et al. **Contractile smooth muscle and active stress generation in porcine common carotids.** *J Biomech Eng.* 2018; **140**(1):1-6.

Zvarova B, Uhl FE, Uriarte JJ, et al. **Residual detergent detection methods for nondestructive cytocompatibility evaluation of decellularized whole lung scaffolds.** *Tissue Eng Part C Methods*. 2016; **22**(5):418-428.